PHYSICAL REVIEW A VOLUME 39, NUMBER 10 MAY 15, 1989

Cooperative dynamics and functions in a collective nonlinear optical element system

Kenju Otsuka
NTT Basic Research Laboratories, Musashino-shi, Tokyo 180, Japan

Kensuke Ikeda
Research Institute for Fundamental Physics, Kyoto University, Kyoto 606, Japan
(Received 28 September 1988)

An optical ring cavity containing distributed nonlinear elements is proposed as a simple metaphorical model for investigating the dynamic properties of spatial chaos in a system far from thermal equilibrium. If the coupling between the elements is unidirectional, the stability of the disordered structure can be determined by the spatial Lyapunov exponent. This fact implies that spatial chaos is almost dynamically unstable and is replaced by spatiotemporal chaos. However, in the case of bidirectional coupling, the spatial chaos is self-induced over a wide range of the control parameter, which means that a memory function is formed cooperatively in the system. We predict several cooperative phenomena and describe their physical origin in terms of nonlinear dynamics. In particular, characteristics of spatial chaos applied to information storage are studied in detail. Applicability of predicted phenomena such as a cooperative all-optical switching, multivibrator operations, flip-flop operations, as well as spatial chaos memory, is discussed.

I. INTRODUCTION

Collective behavior, which arises through the interaction of elemental components, is currently of interest in nonlinear dynamics. Whether these components are neurons, amino acids, and so on, the collective behavior of the whole is qualitatively different from the sum of the individual parts. This concept is referred to as a *Gestalt* from the German philosophical concept that the whole is more than the sum of its parts. In this paper, a nonlinear optical system consisting of distributed nonlinear elements is proposed as a promising candidate for a system which possesses novel collective functions. Our basic perspective is to create cooperative function through the summing of simple elements.

So far, the study of optical systems has been restricted to individual elements, such as lasers and bistable optical elements.[1,2] Of course, research has been done to achieve various types of logic functions by integrating these elements. However, such a design concept is only an extension of the idea of semiconductor integrated circuits to optical systems. In addition, integrated optical logic circuits developed so far are inferior to state-of-art semiconductor logic devices in terms of switching speed. On the other hand, attention has been paid to collective devices consisting of coupled elemental components. This configuration results in automatic parallel processing and intelligent behavior. For example, neural networks and their optical analogue, that is, holographic systems, can function as associative memory.[3,4] If similar intelligent operations can be achieved in the form of parallel processing, the low processing speed of optical devices may be overcome sufficiently. The study of collective functions expected to exist in coupled lasers or nonlinear elements will provide a new insight into practical nonlinear optical devices.

Dynamics of lasers and bistable optical devices are described by simple rules as individual elements. In spite of their simple dynamic rules, these systems have recently been recognized to exhibit dynamic instabilities and complex behaviors,[5] e.g., chaos. Some of these complex dynamic behaviors are applicable to signal processing. However, the collective functions of simple stable elemental components should be studied rather than the unstable behavior of individual elements.

This paper proposes a novel collective optical device which can be implemented using practical nonlinear optical media. The elements of the proposed system consist of a nonlinear dielectric material placed between optical mirrors. An individual element is coupled to an adjacent element by optical beams. If the optical coupling is absent, an individual element does not show any active function. However, the collective elements show very attractive dynamic and static functions as a system when the optical coupling is introduced. The proposed system is interesting in terms of nonlinear dynamics; moreover, it possesses a variety of cooperative functions from the viewpoint of practical application.

Underlying the proposed system is the general problem of spatial disorder (chaos), an important general subject in the field of classical condensed matter. Recently, the origin of spatial disorder has been discussed in relation to the problem of dynamic systems. Recently, Aubry has extensively studied the significance of spatial chaos in an equilibrium system. He elucidated the complex structure of commensurate-incommensurate phase transition in terms of dynamic structure associated with spatial chaos.[6] On the other hand, Yumoto and Otsuka recently predicted the existence of spatial chaos in an externally pumped nonlinear optical system.[7] Since then, several examples of systems which exhibit spatial chaos have been proposed for optical systems.[8,9] In macroscopic

nonequilibrium systems such as externally pumped optical systems, dynamic stability rather than thermodynamic stability plays the essential role. However, the dynamic stability of spatial chaos in nonequilibrium systems has been left an open question.

In the present paper, we discuss the dynamic stability of spatial chaos expected in the proposed distributed optical element system, paying specific attention to the potential applicability of spatial chaos to information storage (memory). In Sec. II the physical background and motivations of this work will be reviewed in connection with the spatial chaos problem. In Sec. III a conceptual model of an optical system with distributed nonlinear elements is described and a fundamental equation which governs the proposed system is introduced. Section IV discusses the bifurcation of spatial solutions and investigates the dynamic stability of these solutions for unidirectional and bidirectional coupling. It is shown that the two different coupling schemes lead to quite different answers to the dynamic stability of spatial chaos. In Sec. V we discuss the applicability of some forms of cooperative behavior that can be expected of the system, such as all-optical switching, and multivibrator and flip-flop operations. In particular, characteristics of spatial chaos are discussed regarding potential applicability of spatial chaos to information storage.

II. PHYSICAL BACKGROUND

An interesting aspect of chaos is that a variety of patterns can be produced even though the production rule is quite simple. Concerning application, we may have two ways of regarding chaos. From the viewpoint that chaos implies complicated uncontrollable dynamic behavior, one may feel that chaos should be avoided since it cannot be predicted. In fact, the majority of workers try to apply knowledge of chaos in order to remove the uncontrollable aspect of the system. If one views chaos from another viewpoint, it acts as an "information generator" which can produce all sorts of possible patterns. From this standpoint, the study of chaos might be encouraged, since it plays the part of an ideal information carrier. Such a viewpoint seems to be supported by only a few workers, including the present authors.[10,11]

The existence of chaos implies that the number of coexisting periodic solutions increases exponentially $\exp(hT)$ with period T, where h is the topological entropy greater than zero. These periodic solutions can be expressed by a binary code in an ideal case and periodic solutions coexist which correspond to all binary series. If these coexisting periodic solutions can be used as a memory, it is basically possible to store information of $\log_2(h)$ bits per unit time in a chaotic system. Recently, Davis and Ikeda proposed that coexisting stable periodic solutions due to complex bifurcation just before chaos in an optical system can be applied to a dynamic memory.[10] A positive role for chaos in switching between different periodic states is also emphasized.[11] Unfortunately, in most cases, these periodic solutions are unstable in the chaotic regime, and make transitions to other periodic solutions in the presence of quite small perturbation. This is reasonable since temporal chaos can be understood in terms of the transition phenomena between unstable periodic solutions.

Another interesting fact exists. If chaos can be generated as spatial patterns instead of temporal patterns, spatial chaos, or more strictly speaking a spatially unstable periodic pattern embedded in the chaotic patterns, seems likely to be temporally stable. Such a possibility has been pointed out by Aubry in a completely different physical context.[6]

Aubry's physical system provides a critical test of chaos memory, and therefore we review his system a little more precisely. Aubry discussed the Frenkel-Kontrova system, which can be expressed by the following Hamiltonian:

$$H=(K/2)(X_{n+1}-X_n)^2+\cos X_n, \quad n=1,2,3,\ldots,N \tag{1}$$

and investigated the spatial structure of the system $\{X_1,X_2,\ldots,X_N\}$ $(X_N=X_1)$. The spatial structure can be expressed as the solutions of the mapping rule obtained by minimizing the Hamiltonian functional (1),

$$X_{n+1}-X_n=p_n/K\ , \tag{2}$$

$$p_{n+1}-p_n=\sin X_{n+1}\ . \tag{3}$$

Equations (2) and (3) are the so-called standard map, and almost all the solutions become chaotic if the coupling constant between the element K becomes smaller than a certain threshold value. He conjectured that such a chaotic solution corresponds to a local minimum of $H\{X_n\}$. More precisely, a large variety of spatially unstable periodic solutions embedded in the chaotic sea are dynamically stable. The simplest example is the spatially unstable period-1 cycle solution given by

$$X_n=\pi, \quad p_n=0\ . \tag{4}$$

If one carries out a linear-stability analysis around this solution, it is easily shown that this solution in fact stands for a local minimum of the system.

At a finite temperature, however, various periodic spatial solutions which construct spatial chaos become metastable since the system can overstep the barrier of local minima thermally. This process is expressed by the following Langevin-type equation:

$$\frac{\partial X_n}{\partial t}=-\frac{\partial H(X_n)}{\partial X_n}+f_n(t)\ . \tag{5}$$

Here, $\langle f_n(t)f_{n'}(t)\rangle=\delta(t-t')\delta_{nn'}\langle f^2\rangle$ is a random force. The random driving force destroys the metastable state. As a consequence, the metastable state has a finite lifetime in Aubry's equilibrium system.

If one intends to make such a lifetime longer such that these solutions can be utilized as a spatial memory, the elemental part X_n should be constructed with a macroscopic system. However, one cannot ensure that such a macroscopic system in general obeys the simple relaxation-type dynamics driven by the force $F_n=\partial H(X_n)/\partial X_n$ derived by the Hamiltonian functional in Eq. (5). In particular, in nonequilibrium macroscopic

systems, there is in general no need to satisfy the following potential condition:

$$\frac{\partial F_n}{\partial X_{n'}} = \frac{\partial F_{n'}}{\partial X_n} . \tag{6}$$

In a macroscopic nonequilibrium system, the dynamics cannot in general be expressed in terms of the relaxation process towards local minima given by Eq. (5). Under this situation, however, it seems to be rather difficult to realize spatial chaos as frozen spatial patterns and the possibility arises that spatial chaos is replaced by turbulence (spatiotemporal chaos) due to dynamic instability.

The first question then arises: Is spatial chaos dynamically stable in macroscopic nonequilibrium systems? The possibility of the existence of spatial chaos in nonequilibrium systems has been proposed by Yumoto and Otsuka.[7] They pointed out that the polarization state of light changes chaotically in a nonlinear-refractive-index medium which is excited by counterpropagating beams (degenerate four-wave mixing scheme). If these spatial chaos solutions are dynamically stable, their system becomes an ideal candidate for realizing spatial chaos memory. Unfortunately, the dynamic analysis of their system is very difficult and no information has been obtained regarding its dynamic stability.

Let us go back to Aubry's system again. Aubry's system can be interpreted as an assembly of elements each of which has the on-site potential $V(X_n)=\cos X_n$. The existence of local minima of on-site potential means that each element has a memory capacity. In the limit of small coupling $K \rightarrow 0$ between the elements, any structure in which the states of each element are arranged randomly on the potential $X_n = 2\pi k_n$ (n is an integer) appears to be stable. Such structures are the random limit of spatial chaos solutions. Therefore the memory capacity per unit element provided by the most random spatial chaos is equal to the number of local minima of each element. The memory capacity does not decrease very much even if coupling between the elements is introduced. Firth claimed along this line that diffusive coupling (cross talk) between optically bistable pixels does not drastically decrease the memory capacity of pixel arrays.[9] However, in a system in which spatial chaos is ensured by the existence of many local minima in "on-site" potential of decoupled elements, the memory capacity should rather be decreased due to the coupling between elements. Our perspective is to increase the memory capacity drastically by introducing spatial chaos into the system by coupling simple elements which individually do not have local minima, i.e., memory capacity. The second question then arises: Is it possible to realize spatial chaos in a collective system when elements which have no memory function are coupled to each other by a suitable coupling mechanism? Even though the answers to the two issues mentioned above are positive, there still remains a basic question concerning the possibility of controlling the spatial chaos as memory: Can spatial chaos memory be addressed easily? In particular, is it possible to switch between spatial chaos patterns by external control?

If the answers to the above questions are positive, then we can construct a memory device by summing simple elemental parts. That is the "cooperative formation of memory functions." The main subject of this paper is to investigate the above three issues. We will show that such a spatial chaos memory device can be realized by a collective nonlinear optical element system.[12] Although the configuration of the proposed system is rather complex and is not appropriate for practical use, it is very convenient for examining the memory function of spatial chaos. In this sense, the proposed model can be considered as a metaphorical model of spatial chaos memory.

III. MODEL

In the conceptual model of the proposed system shown in Fig. 1, nonlinear elements possessing third-order susceptibility are arranged in an optical ring cavity. These elements interact via counterpropagating light beams $(A_F^{(k)}, A_B^{(k)})$ that are introduced through the mirrors which separate the elements. The forward and backward propagating waves couple through the nonlinear refractive index grating formed in the medium. This effect makes the analysis quite difficult. Therefore we assume that the refractive-index grating diffuses very fast and we neglect the mutual coupling through the refractive-index grating. Then the Maxwell-Debye (or Bloch) equation which describes the motion of electric fields $E_F^{(k)}, E_B^{(k)}$ and the nonlinear phase shift introduced into the electric field at each cell $\phi_F^{(k)}, \phi_B^{(k)}$ can be reduced to the following delay differential equations:

$$E_F^{(k)}(t+t_R) = A_F^{(k)} + B \exp\{i[\phi_F^{(k-1)}(t) + \phi_0^{(k-1)}]\} E_F^{(k-1)}(t) , \tag{7}$$

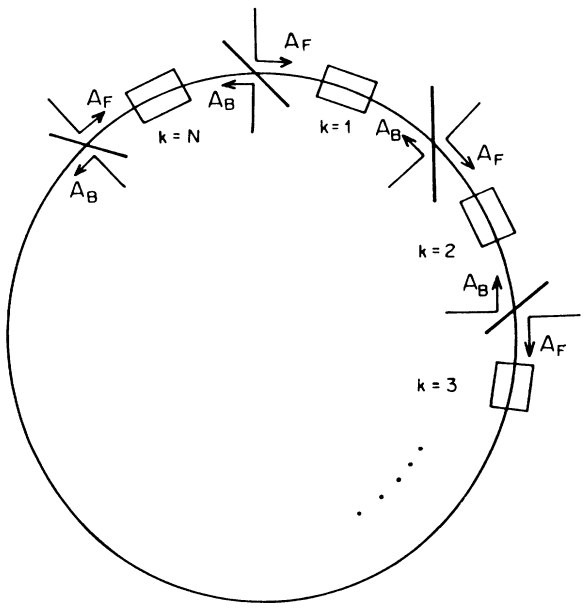

FIG. 1. Conceptual model of a nonlinear optical system with distributed nonlinear elements.

$$E_B^{(k)}(t+t_R)=A_B^{(k)}+B\exp\{i[\phi_B^{(k+1)}(t)+\phi_0^{(k+1)}]\}E_B^{(k+1)}(t)\ , \quad (8)$$

$$\tau(\partial\phi_F^{(k)}(t)/\partial t)=-\phi_F^{(k)}(t)+q[(1-e^{-\alpha l})/\alpha]|E_F^{(k)}(t)|^2+q\int_0^l ds\, e^{-\alpha s}|E_B^{(k)}(t+l/c-2s/c)|^2\ , \quad (9)$$

$$\tau(\partial\phi_B^{(k)}(t)/\partial t)=-\phi_B^{(k)}(t)+q[(1-e^{-\alpha l})/\alpha]|E_B^{(k)}(t)|^2+q\int_0^l ds\, e^{-\alpha s}|E_F^{(k)}(t+l/c-2s/c)|^2\ . \quad (10)$$

Here, c is the velocity of light, $B=\sqrt{R}\,e^{-\alpha l/2}$ is the coupling coefficient between the adjacent cells (R is the mirror reflectivity, α the absorption coefficient, and l the cell length), $\phi_0^{(k)}$ is the linear phase shift across the kth cell, and $q\equiv\mathrm{sgn}(n_2)[\alpha/(1-e^{-\alpha l})]$ (n_2 is the quadratic coefficient of the nonlinear refractive index). The derivations of these equations are given in Appendix A.

To extract the essence of a coupled element system, let us simplify these equations further. First, we assume that the variation of the electric field intensity during the transit time through the cell is negligible, i.e., $t_R=l/c,\to 0$. Next, we assume that absorption by the medium is negligible, i.e., $\alpha l\to 0$. Then, Eqs. (9) and (10) reduce to

$$\tau(\partial\phi_F^{(k)}(t)/\partial t)=-\phi_F^{(k)}(t)+|E_F^{(k)}(t)|^2+|E_B^{(k)}(t)|^2\ , \quad (11)$$

$$\tau(\partial\phi_B^{(k)}(t)/\partial t)=-\phi_B^{(k)}(t)+|E_F^{(k)}(t)|^2+|E_B^{(k)}(t)|^2\ . \quad (12)$$

Since $\tau(\partial\phi_F^{(k)}(t)/\partial t-\partial\phi_B^{(k)}(t)/\partial t)=-(\phi_F^{(k)}(t)-\phi_B^{(k)}(t))$, the term $|\phi_F^{(k)}(t)-\phi_B^{(k)}(t)|$ goes to zero asymptotically. Thus we may set $\phi_F^{(k)}(t)=\phi_B^{(k)}(t)\equiv\phi_k(t)$.

We consider the limit of large dissipation, i.e., $B=\sqrt{R}\ll 1$ with $A_{F,B}^{(k)2}B\sim O(1)$.[13] Then, from Eqs. (7) and (8), the field intensities at the kth cell are expressed as

$$f_F^{(k)}(\phi_{k-1})\equiv|E_F^{(k)}(t)|^2=A_F^{(k)2}\{1+2B\eta_F^{(k)}\cos[\phi_{k-1}(t)+\phi_0^{(k-1)}]\}\ , \quad (13)$$

$$f_B^{(k)}(\phi_{k+1})\equiv|E_B^{(k)}(t)|^2=A_B^{(k)2}\{1+2B\eta_B^{(k)}\cos[\phi_{k+1}(t)+\phi_0^{(k+1)}]\}\ , \quad (14)$$

with

$$\eta_F^{(k)}=A_F^{(k-1)}/A_F^{(k)},\quad \eta_B^{(k)}=A_B^{(k+1)}/A_B^{(k)}\ .$$

The dynamics of nonlinear phase shift $\phi_k(t)\equiv\phi_F^{(k)}(t)=\phi_B^{(k)}(t)$ thus obey a simpler dynamic equation,

$$\tau\dot{\phi}_k=-\phi_k+f_F^{(k)}(\phi_{k-1})+f_B^{(k)}(\phi_{k+1})\ . \quad (15)$$

Henceforth we often consider the ideal case in which the input fields as well as the linear phase shift do not depend on the cell, i.e., $A_F^{(k)}=A_F$, $A_B^{(k)}=A_B$, $\phi_0^{(k)}=\phi_0$. In such a case, superscript (k) in the nearest-neighbor coupling forces in Eqs. (13)–(15) can be discarded and the dynamics of the system obey the following simple equation of motion:

$$\tau\dot{\phi}_k=-\phi_k+f_F(\phi_{k-1})+f_B(\phi_{k+1})\ , \quad (16)$$

with

$$f_{F,B}(\phi_k)\equiv A_{F,B}^2[1+2B\cos(\phi_k+\phi_0)]\ . \quad (17)$$

The analyses in the following sections are based on model equations (13)–(15) or (16) and (17).

IV. SPATIAL BIFURCATION AND DYNAMIC STABILITY

A. Unidirectional coupling

First let us consider the case of undirectional coupling, i.e., $A_F^{(k)}=A$ and $A_B^{(k)}=0$ and examine the dynamic stability of stationary spatial structures. In this case, the stationary solution $\bar{\phi}_k$ of Eq. (16) is determined by the mapping rule

$$\bar{\phi}_{k+1}=f_F(\bar{\phi}_k)\ . \quad (18)$$

The properties of the solutions of mapping rule Eq. (18) are well investigated.[14] In particular, the solution is shown to exhibit complicated bifurcation phenomena when the nonlinear parameter, that is, A^2 in our case, is changed. The spatial structure which can exist in our case are those whose spatial period is N or its divisor that satisfy the following boundary condition:

$$\bar{\phi}_{N+1}=\bar{\phi}_1\ . \quad (19)$$

However, let us forget this restriction for a moment and look at the bifurcation phenomena based on Eq. (18).

There are three types of solutions in Eq. (18), namely, stable periodic solutions, unstable periodic solutions, and nonperiodic solutions. Among the solutions which can be obtained by iterating the map Eq. (18), only stable periodic solutions and observable nonperiodic solutions (i.e., chaotic solutions) can be seen. The result is shown in Fig. 2(a) assuming $B=0.1$ and $\phi_0=0$. Unstable periodic solutions and nonobservable nonperiodic solutions are not seen in this figure, however, the global behavior can be understood. In short, the stable period one cycle solution exhibits successive spatial period-doubling bifurcations leading to spatial chaos. Within the chaotic regime, a lot of stable periodic solutions whose period $p\neq 1$ are embedded as windows.

Among these solutions, spatial solutions which satisfy the boundary condition of Eq. (19) and are dynamically stable can exist as stable structures. The dynamical stability of these solutions can be examined by the linear-stability analysis of Eqs. (16) and (17). The spectrum of the small deviation around the stationary solutions $\delta\phi_k=\delta\bar{\phi}_k\exp(\lambda t)$ is governed by the following characteristic equation:

$$(\lambda+1)^N=\exp(N\alpha)\mathrm{sgn}\sigma,\quad \sigma=\prod_{k=1}^{N} f_F'(\bar{\phi}_k)\ , \quad (20)$$

where

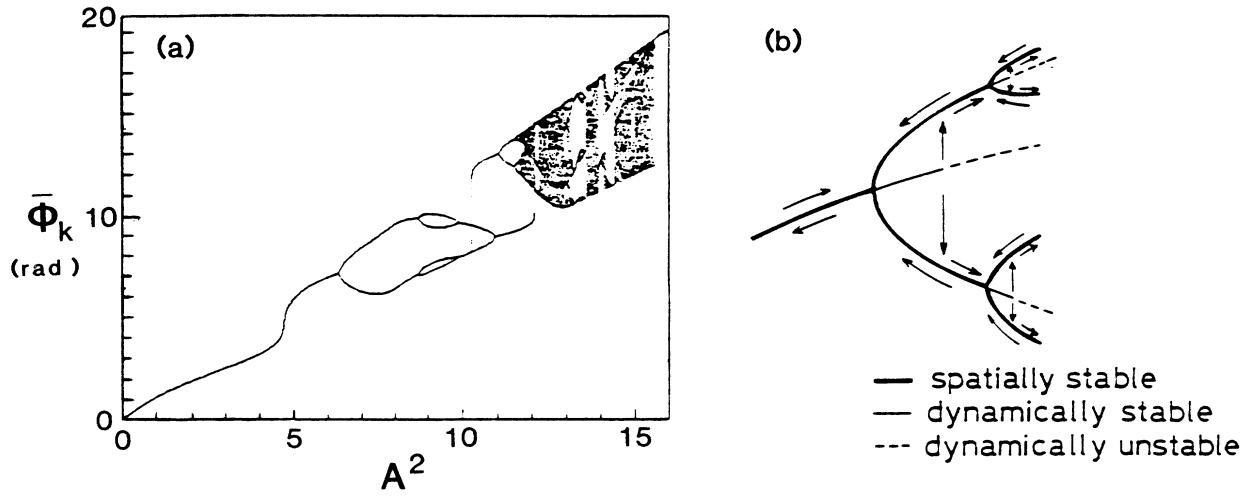

FIG. 2. (a) Bifurcation diagram for $\phi_0=0$ and $B=0.1$. (b) Realized process of spatial bifurcation by increasing or decreasing input parameter A^2.

$$\alpha=(1/N)\sum_{k=1}^{N}\ln|f_F'(\bar{\phi}_k)| \tag{21}$$

is the "spatial Lyapunov exponent" of the periodic solutions of $\bar{\phi}_1,\bar{\phi}_2,\ldots,\bar{\phi}_N$. Obviously, the structures whose $\alpha<0$ correspond to the "stable" periodic solutions of Eq. (18) and the structures whose $\alpha>0$ correspond to "unstable" periodic solutions of Eq. (18). The structures of $\alpha<0$ (>0) are referred to as *spatially* stable (unstable) structures hereafter. The existence of spatially unstable structures implies that the number of spatial structures increases exponentially with the system size N. Therefore the sign of the spatial Lyapunov exponent and the dynamic stability of the structures are extremely crucial as criteria of whether the latent memory capacity is positive or zero, as was discussed in Sec. II. Equation (20) indicates that the *dynamic* stability of the structures are closely related to the *spatial* stability. The solutions of Eq. (20) are given by

$$\lambda=-1+\exp(\alpha)\exp(i2n\pi/N)\quad(\sigma>0)\,, \tag{22a}$$

$$\lambda=-1+\exp(\alpha)\exp[-i(2n\pi+\pi)/N]\quad(\sigma<0)\,. \tag{22b}$$

Therefore the spatially stable structures, e.g., $\alpha<0$, are dynamically stable since all real $\lambda<0$. Even if α becomes positive through spatial bifurcations, when $\sigma<0$, i.e., the bifurcation is an inverted type, all real λ are found to become negative for $0<\alpha<\ln|1/\cos(\pi/N)|$.

This means that if a spatially stable period-p cycle structure is realized, period-doubled structures $p\times2, p\times2^2, \ldots$ which are born through the inverted bifurcation from the period-p cycle structure are shown to exhibit a dynamically stable transition by the continuous change in A^2. This process is depicted in Fig. 2(b).

Now, let us discuss the dynamic stability domain of realizable spatial structures from the global viewpoint. As has been discussed so far, the dynamic stability

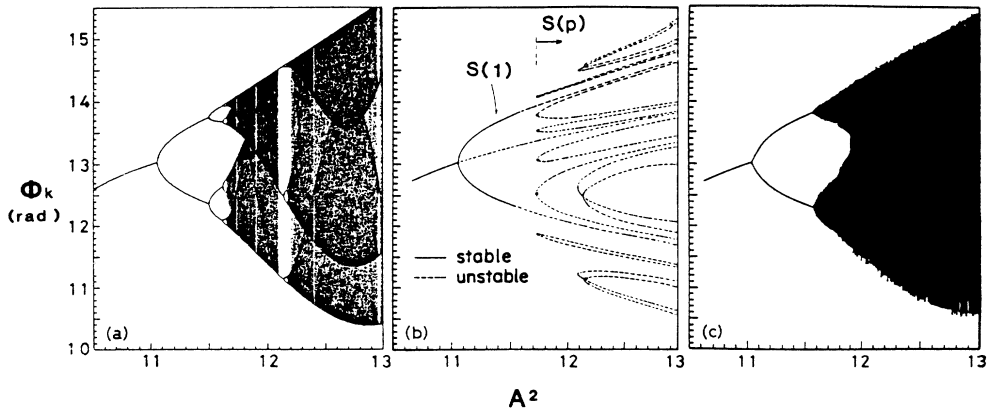

FIG. 3. (a) Iterative solution for $N=6$, $B=0.1$, and $\phi_0=0$. (b) Stationary solution as a function of A^2. Solid and dotted curves correspond to dynamically stable and unstable solutions, respectively. (c) $\phi_k(t)$ $(k=1,2,\ldots,6)$ vs A^2.

domain roughly coincides with the spatial stability domain in the case of $N \gg 1$. The spatial stability domain is nothing more than the stable periodic solutions of the map Eq. (18). As a consequence, realizable spatial structures include the period-1 cycle solution, its period-doubled solutions (2^n) and period-p cycle solutions as well as their period-doubled solutions $p \times 2^n$, which are embedded as windows as shown in Fig. 2(a). The stability domain of these windows becomes narrower exponentially as p increases and therefore it is negligibly small for large-p values.

Let us explain the stability domain further for the case of $N=3\times 2$. In this case periodic structures of period 1, 2, 3, and 6 can exist. Figure 3(b) depicts the bifurcation structure which gives all the possible stable and unstable periodic solutions. It is easy to see that there are two classes of periodic structures. One implies the period-1 cycle solution connected to the trivial solution of $\bar{\phi}_k=0$ as $A\to 0$, and 1×2^n cycle solutions period doubled from the period-1 cycle solution. This sequence is referred to as $S(1)$. The other class of solution consists of period-N and period-p cycle solutions (p is any integer $\neq 1,N$) which appear via tangential bifurcation, and $p\times 2^n$ cycle solutions period doubled from the period-p cycle solutions. This sequence is referred to as $S(p)$. As for $N=6$, $S(6)$ and $S(3)$ are realized. From the viewpoint of the map solution of Eq. (18) [Fig. 3(a)], the stable branches which are shown by solid lines in Fig. 3(b) are observed as window phenomena of the map solution. These dynamically stable domains, which are born via tangential bifurcations, are isolated from each other and the stable domain of longer-period solutions, for instance $S(6)$, becomes narrower exponentially.

The problem here is the connectivity between these isolated stability domains. Does the $S(1)$ structure connect to the $S(6)$ or $S(3)$ structures by increasing A^2 continuously? This is not the case. $S(6)$ and $S(3)$ [generally $S(p(\neq 1))$] form isolas as is seen in Fig. 3(b) and they are of course isolated from $S(1)$ as well as from other isolas. In fact, these window structures are isolated and are found from the computer experiment not to connect to $S(1)$ by the continuous increase in A^2. Such a manner is shown in Fig. 3(c), where $\phi_k(t)$ ($k=1,2,\ldots,6$) are plotted as A^2 is increased very slowly. Now, let us start from the $S(1)$ structure. Since $N=6$, the period-2 cycle structure belonging to $S(1)$ appears as a dynamically stable structure at first. As A^2 is increased, the stationary solutions exhibit instability and make a transition to spatiotemporal chaos (STC) through periodic oscillating solutions. This solution exists even when A^2 reaches the stability domains of $S(6)$ and $S(3)$. In other words, $S(p)$ ($p=3$ or 6) coexist with STC, which is generated from $S(1)$. In addition, the computer experiment indicates that the basin of attraction of $S(p(\neq 1))$ is extremely small compared with that of the temporally varying solutions. Roughly speaking, the size of the basin of attraction is proportional to the scale of the domain of dynamic stability.

The complicated spatial structures with long periods are almost impossible to realize with unidirectional coupling. The stability domain of realizable structures is ex-

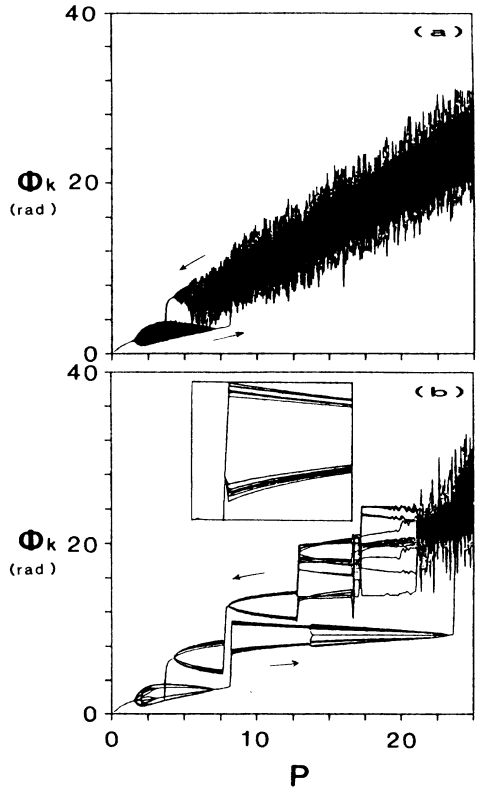

FIG. 4. $\phi_k(t)$ ($k=1,2,\ldots,N$) vs P. $B=0.3$, $\phi_0=0$, and $N=23$. (a) Unidirectional, (b) bidirectional. Inset: Enlargement around $P=10$. In this case, symmetric period-N solutions are realized and "multifurcation" into 12 different states is seen.

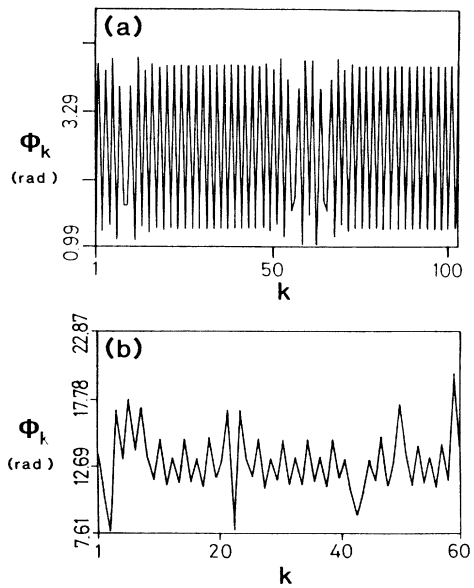

FIG. 5. Typical patterns of spatial multifurcated structure. (a) For the low-P regime: $P=3.2$, $N=103$, $B=0.5$, $\phi_0=0$. (b) For the high-P regime: $P=11.18$, $N=60$, $B=0.5$, and $\phi_0=0$.

tremely narrow and the basin of attraction is extremely small. In addition, the realizable solutions are almost spatially stable, thus they are not spatial chaos. The spatial chaos is dynamically unstable and is converted into spatiotemporal chaos in the unidirectional coupling scheme. In other words, all the spatially unstable patterns, which are expected to possess a finite memory capacity, are dynamically unstable. Therefore the actual memory capacity in the unidirectional coupling scheme is zero. However, a dramatic change takes place in the case of bidirectional coupling, which will be discussed in Sec. IV B.

The unidirectional coupling scheme is not so interesting as a means of realizing spatial chaos, i.e., information storage. However, this scheme can provide interesting cooperative phenomena as will be described later in Sec. V A.

B. Bidirectional coupling

Next, let us consider the case of bidirectional coupling where $A_F^{(k)}=A_B^{(k)}=A$. In this case, the dynamics are dramatically changed. Although the interactions between the nearest-neighbor cells are symmetric, Eq. (16) lacks the potential condition of $\partial\dot{\phi}_k/\partial\phi_{k-1}=\partial\dot{\phi}_{k-1}/\partial\phi_k$, and thus there is no Lyapunov functional which corresponds to a Hamiltonian (or free energy) in equilibrium systems. Therefore one cannot ensure an approach to static configurations. Indeed, STC takes place in a regime of quite high intensity ($P=A_F^2+A_B^2$). In contrast to the unidirectional case, however, self-induced spatial disorder is found to be stabilized over wide regions. Here, we first show an example of numerical simulation. The ϕ_k are plotted, except for transients, as P is increased (or decreased) very slowly in time in the case of bidirectional coupling [Fig. 4(b)]. We see that ϕ_k varies stepwise with P, being accompanied by hysteresis, although the STC appears on the higher intensity side ($P\geq 20$). On the low-intensity side of each step, ϕ_k is multifurcated into N different static values. This multifurcation implies that the spatial distribution of ϕ_k is frozen into a state with different values at different sites. Moreover, the global structure of hysteresis as well as of bifurcation does not depend on the system. (We examined systems of size up to 711.) The inset is an enlargement around the input intensity of $P=10$. Since Eq. (16) does not have a Lyapunov functional, it is very difficult to judge rigorously whether the N-period cycle solution is really the "ground state" or not. Two typical patterns of spatially multifurcated structure are depicted in Fig. 5. These are obtained for low-P ($P=3.2$) and high-P ($P=11.18$) regimes. In the low-P side, the spatial structure looks almost like a period-2 cycle pattern into which "defectlike" structures are inserted. In the high-P side, the spatial structure is quite irregular, but it seems to wander between different period-2 cycle structures. Therefore let us then look at the stable domain of period-2 cycle solutions which forms a basis for the "multifurcated" structure.

Stationary solutions for the bidirectional case are determined by the following rule, which corresponds to Eqs. (18) and (19) for the unidirectional case,

$$\bar{\phi}_k=f_F(\bar{\phi}_{k-1})+f_B(\bar{\phi}_{k+1}),\quad \bar{\phi}_1=\bar{\phi}_{N+1}\ . \tag{23}$$

This rule defines the following two-dimensional mapping rule, which determines $\bar{\Phi}_{k+1}\equiv(\bar{\phi}_{k+1},\bar{\phi}_k)$ from $\bar{\Phi}_k\equiv(\bar{\phi}_k,\bar{\phi}_{k-1})$:

$$\mathbf{F}:(\bar{\phi}_k,\bar{\phi}_{k-1})\mapsto(\bar{\phi}_{k+1},\bar{\phi}_k)=(f_B^{-1}(\bar{\phi}_k-f_F(\bar{\phi}_{k-1})),\bar{\phi}_k)\ . \tag{24}$$

Here, "spatial instability" is used to imply that a positive Lyapunov exponent exists in the dynamic system along the spatial structure $(\bar{\phi}_1,\bar{\phi}_2,\ldots)$. On the other hand, the "dynamic stability" of the spatial structure $(\bar{\phi}_1,\bar{\phi}_2,\ldots)$ is determined by the sign of roots (λ) of the following linearlized characteristic equation for the small deviation around the stationary solutions $\delta\phi_k=\delta\tilde{\phi}_k\exp(\lambda t)$:

$$\tau\lambda\delta\tilde{\phi}_k=-\delta\tilde{\phi}_k+f_F'(\bar{\phi}_{k-1})\delta\tilde{\phi}_{k-1}+f_B'(\bar{\phi}_{k+1})\delta\tilde{\phi}_{k+1}\ . \tag{25}$$

Here, we introduce the function

$$f_F(\phi)=f_B(\phi)\equiv\tfrac{1}{2}f_P(\phi)\ . \tag{26}$$

When $P\equiv A_F^2+A_B^2$ is small, the period-1 cycle solution $\bar{\phi}_k=x_1$ satisfying $x_1=f_P(x_1)$ is a stable structure. However, the period-1 cycle structure becomes dynamically unstable and bifurcation takes place as P exceeds the critical value P_c. In this regime, the period-2 cycle structure $\bar{\phi}_{2k-1}$(or $\bar{\phi}_{2k}$)$=x_1$, and $\bar{\phi}_{2k}$(or $\bar{\phi}_{2k-1}$)$=x_2$, which is determined by $x_1=f_P(x_2)$ and $x_2=f_P(x_1)$, is realized similarly to the unidirectional case. The dynamic stability of these period-2 cycle solutions is found to be greatly different from that for the unidirectional case. Let us examine the dynamic stability index λ for two coupling schemes, assuming N (cell number) is even. From a simple analysis of Eq. (25), the following equations are given:

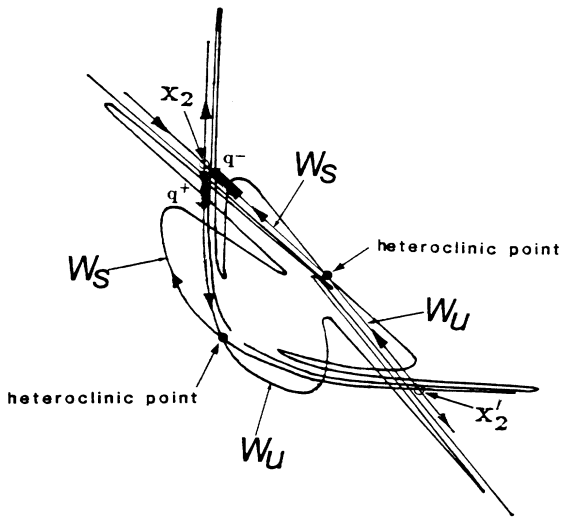

FIG. 6. Schematic illustration of a heteroclinic crossing.

(1) $S \equiv f'(x_1)f'(x_2) > 0$,

$$\lambda = \begin{cases} -1 + \frac{1}{2}|S|^{1/2}\cos(\theta/2) & \text{(bidirectional)} \quad (27) \\ -1 + |S|^{1/2}\exp(i\theta/2) & \text{(unidirectional);} \quad (28) \end{cases}$$

(2) $S < 0$

$$\lambda = \begin{cases} -1 + \frac{1}{2}|S|^{1/2} i \cos(\theta/2) & \text{(bidirectional),} \quad (29) \\ -1 + |S|^{1/2} i \exp(i\theta/2) & \text{(unidirectional);} \quad (30) \end{cases}$$

where $\theta = 2k\pi/N$ $(k = 0, 1, 2, \ldots, N)$.

As for the unidirectional case, the dynamically stable region ($\lambda < 0$) almost coincides with the region of $|S| < 1$ where the period-2 cycle solutions are spatially stable. As a result, the region where the period-2 cycle solutions are realized is extremely narrow as was described in Sec. IV A. In the bidirectional scheme, the situation drastically changes. In short, the period-2 cycle structures become dynamically stable ($\lambda < 0$) even in the spatially unstable region; when P is increased, S first reaches 1 and the period-2 cycle structure appears at this point. This structure is stable following Eq. (27). When P is increased further, S increases in a negative direction. The period-2 cycle structure in the unidirectional case becomes unstable when S becomes smaller than -1 due to Eq. (30). In the bidirectional case, to the contrary, the period-2 cycle structure is dynamically stable even when it is spatially destabilized, i.e., $S < -1$. [See Eq. (29).] This fact implies that the local feedback due to the bidirectional coupling much stabilizes the period-2 cycle structure.

1. *Spatial heteroclinic structure*

The fact that the spatially unstable period-2 cycle structures can exist stably in time is the key to the existence of spatial chaos. The period-2 cycle structure is represented by two-dimensional vectors $\mathbf{x}_2 = (x_1, x_2)$ and $\mathbf{x}_2' = (x_2, x_1)$, which are both the fixed points of the second iteration of the spatial evolution rule $\Phi'' = \mathbf{F}(\mathbf{F}(\Phi))$. The spatial instability means that the spatial evolution of a small deviation $\delta\Phi$ ($= \Phi - \mathbf{x}_2$ or $\Phi - \mathbf{x}_2'$) from the period-2 fixed point (i.e., $\Phi = \mathbf{x}_2$ or $\mathbf{x}_2'$) of the second iteration $\Phi'' = \mathbf{F}(\mathbf{F}(\Phi))$ separates from $\mathbf{x}_2$ or

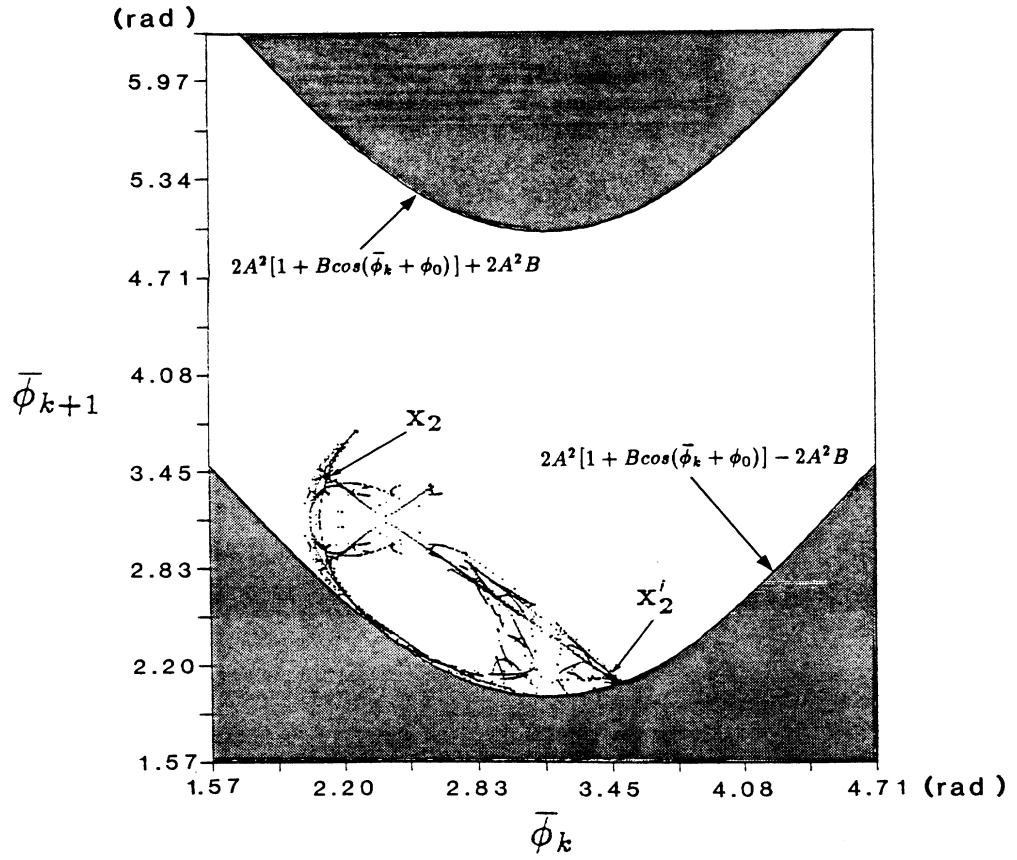

FIG. 7. Heteroclinic complex computed numerically based on the recursive relation of Eq. (24), where $P = 5$, $B = 0.3$, and $\phi_0 = 0$. Solutions cannot exist in the shadowed regions, since $-1 \le \cos(\bar{\phi}_{k+2} + \phi_0) \le 1$. This structure is obtained by choosing the appropriate branch from among mapping solutions physically. Therefore this structure is considered to form part of the actual heteroclinic complex.

$\mathbf{x}_2'$ such that $\delta\phi_k \propto \exp(\nu^+ k)$. Here, the second iteration is determined from Eq. (24) and ν^+ ($|\nu^+|>1$) is one of the two characteristic roots of the following variational equation:

$$\delta\Phi'' = \left.\frac{\partial \mathbf{F}(\mathbf{F}(\Phi))}{\partial \Phi}\right|_{\Phi=\mathbf{x}_2} \delta\Phi \equiv \mathbf{G}\delta\Phi \ . \tag{31}$$

The spatial instability (i.e., $|\nu^+|>1$) takes place only for a real root. Since $\det\mathbf{G}=1$, there is another root ν^- ($|\nu^-|<1$). Therefore $\mathbf{x}_2$ ($\mathbf{x}_2'$) is a hyperbolic fixed point accompanied by manifolds W_u and W_s passing through it (Fig. 6). Consider the motion of the vector Φ governed by the second iteration $\Phi''=\mathbf{F}(\mathbf{F}(\Phi))$. The vector Φ approaches $\mathbf{x}_2$ ($\mathbf{x}_2'$) along W_s, whereas it separates from $\mathbf{x}_2$ ($\mathbf{x}_2'$) along W_u. In the vicinity of $\mathbf{x}_2$ ($\mathbf{x}_2'$), W_u and W_s are in the directions of eigenvectors $\mathbf{q}^{\pm}$ corresponding to the two roots $\mathbf{G}\mathbf{q}^{\pm}=\nu^{\pm}\mathbf{q}^{\pm}$. Manifolds W_u and W_s are called the unstable and stable manifolds. If W_u of $\mathbf{x}_2$ and W_s of $\mathbf{x}_2'$ cross transversally, a so-called heteroclinic orbit is produced and the orbit of the second iteration $\Phi''=\mathbf{F}(\mathbf{F}(\Phi))$ near $\mathbf{x}_2$ and $\mathbf{x}_2'$ is expected to exhibit extremely complex (i.e., chaotic) behavior.[15]

Does a heteroclinic crossing take place in our system? To investigate this problem, the two manifolds W_s and W_u should be determined from Eq. (24). It is easily found that $\mathbf{F}$ is formally multivalued since it includes an inverted function f_P^{-1}. Therefore we chose the branch by appropriate physical selection. The result of numerical computation is shown in Fig. 7. It is apparent that W_u of $\mathbf{x}_2$ crosses W_s of $\mathbf{x}_2'$ and the complex of W_u and W_s forms a multifolded complicated structure. This indicates that heteroclinic chaos appears as a spatial structure. Moreover, since $\mathbf{x}_2$ and $\mathbf{x}_2'$ are dynamically stable, the spatial structure which corresponds to heteroclinic chaos is expected to be stable in time.

What kind of spatial pattern does this heteroclinic orbit produce? A state vector Φ starts from the neighborhood of $\mathbf{x}_2$, and separates from $\mathbf{x}_2$ along W_u and switches to W_s, finally approaching $\mathbf{x}_2'$. Since $\mathbf{x}_2'$ is a hyperbolic fixed point, Φ is repelled by $\mathbf{x}_2'$ and separates from $\mathbf{x}_2'$ along W_u. Thus the heteroclinic orbit indicates the existence of a spatial structure which switches between $\mathbf{x}_2$ and $\mathbf{x}_2'$ chaotically in the manner $\mathbf{x}_2 \rightarrow \mathbf{x}_2' \rightarrow \mathbf{x}_2 \rightarrow \cdots$ The switch from $\mathbf{x}_2$ to $\mathbf{x}_2'$ corresponds to the "defect" shown in Fig. 5. Figure 8 is an enlargement of the defect. The defect is considered to be the interface, i.e., "kink," which connects two types of period-2 cycle structures.

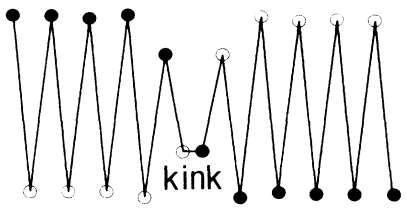

FIG. 8. Enlargement of the "defect" structure.

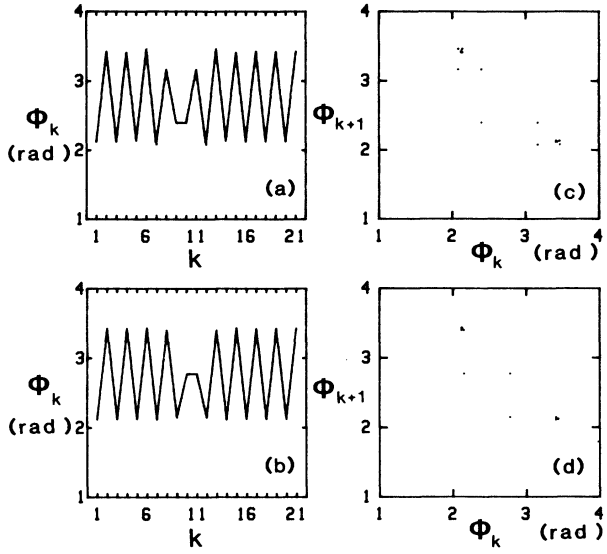

FIG. 9. Two types of "kink" structures for $N=21$, $P=5.0$, $B=0.3$, and $\phi_0=0$. (a) and (b) spatial arrangement of (a) a-type and (b) b-type kinks; (c) and (d) spatial return map.

2. *Stability of heteroclinic chaos structures*

The heteroclinic orbit ensures the existence of a variety of structures including periodic structures. However, these structures are not always dynamically stable. A good example is the two types of kinks shown in Fig. 9. These kinks are stationary solutions of Eq. (23) and the a-type kink is found to be temporally stable. On the other hand, the b-type kink is not temporally stable. It is an intermediate structure when the center of the a-type kink shifts by two lattice sites, as shown in Fig. 10. (Note that

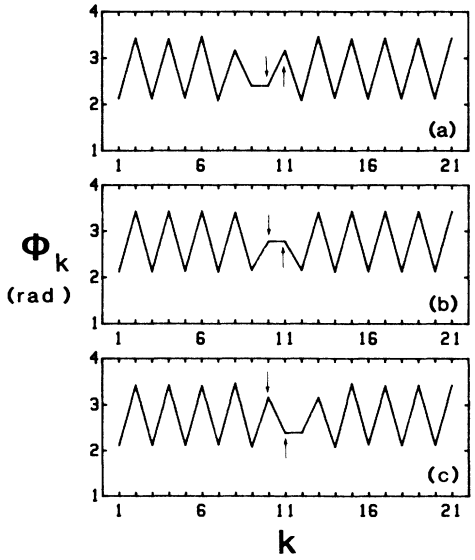

FIG. 10. Relation between a-type and b-type kink structures. (a) a-type kink structure, (b) b-type kink structure, (c) two-lattice site shifted a-type kink structure. $N=21$, $P=5.0$, $B=0.3$, and $\phi_0=0$. b-type kink structure appears on the way from (a) to (c).

two lattice sites comprise a fundamental unit for the movement of kinks.) The motion of our system is expressed by an orbit in N-dimensional phase space $(\phi_1,\phi_2,\ldots,\phi_N)$. We call this space Γ space hereafter. The a-type kink is a stable fixed point in the Γ space. Another a-type kink whose position shifts by two lattice sites [see Fig. 10(c)] is also a stable fixed point. The b-type kink corresponds to an unstable saddle point along a path which connects these two fixed points in the Γ space. Let us actually show evidence of the fact that the b-type kink forms a saddle point. In the transition process (a kink)$\rightarrow$(b kink)$\rightarrow$(a kink), two cells are subjected to the largest change. They are ϕ_{10} and ϕ_{11}, indicated by arrows in the case of Fig. 10. Now, we rewrite them as ϕ_1 and ϕ_2, respectively, and observe the motion in the Γ space projected on this two-dimensional plane (ϕ_1,ϕ_2). Let us first deviate only ϕ_1,ϕ_2 from the a-type kink state and then observe the temporal evolution of the projected motion. The obtained flow lines are shown in Fig. 11. There exists a saddle between the two a-kink states [Figs. 10(a) and 10(c)] indicated by a and a', and this saddle corresponds to b-kink state [Fig. 10(b)]. The motion at first rapidly relaxes toward a slow manifold, which is a straight line connecting a, b, and a', and then relaxes slowly along this manifold toward a or a'. As a result, this manifold is nothing more than a steepest descent from a to a' (or a' to a). In Sec. V B, this steepest descent will be shown to play an important role for switching between chaotic patterns. As is shown in the following, the a-type kink is considered to be a fundamental unit in spatial chaos. Therefore we simply call this structure "kink" hereafter.

The period-2 cycle structures are not realized when N is odd. The period-2 cycle structures into which at least one kink is inserted are realized instead. Let us investigate what type of spatial structures are dynamically stable. To examine this, we made the following numerical experiment. The system is first set to the regime where P is small and the trivial period-1 cycle solution is stable. Then P is increased to the point where period-2 cycle structure appears by adding a small noise randomly in time and space to the linear phase shift ($\phi_0^{(k)}$) or to input electric field ($A_F^{(k)2}$ or $A_B^{(k)2}$) as a seed. After that,

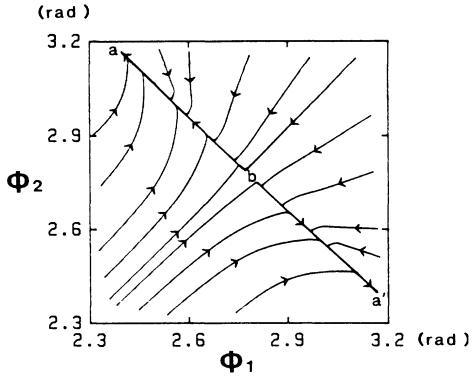

FIG. 11. Flow lines projected on (ϕ_1,ϕ_2) plane. $N=21$, $P=5.0$, $B=0.3$, and $\phi_0=0$.

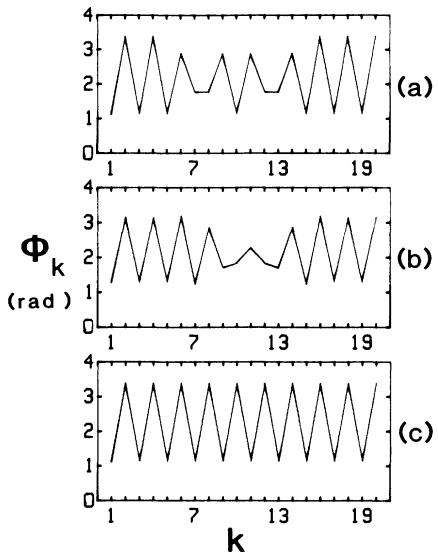

FIG. 12. Spatial arrangement indicating the minimum distance between kinks. $N=21$, $P=2.7$, $B=0.3$, and $\phi_0=0$.

the system is left alone for a long period of time and surviving stable patterns are observed. We call this method "noise-seeded bifurcation." During the transition process from period-1 to period-2 cycle structures, various heteroclinic chaos patterns can be obtained instead of period-2 cycle structures due to the effect of external noise. From the observation of surviving patterns, the following empirical rule is obtained.

Rule. Surviving stable structures are structures where kinks are inserted into period-2 cycle patterns and the distance between kinks is sufficiently large.

Then, how high can we increase the density of kinks in the present system? The approach to this problem is to evaluate the distance at which the kink pair can coexist. Let us consider the arrangement of two kinks as shown in Fig. 12(a). To decrease the distance between kinks and obtain the kink configuration shown in Fig. 12(b), one of the kinks should be shifted by two lattice sites. This means that the system must pass through the saddle point in the Γ space which corresponds to a b-type kink

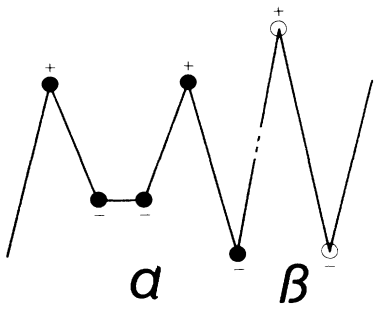

FIG. 13. Fundamental structures which construct dynamically stable heteroclinic structures. $+--+-$, α structure and $+-$, β structure.

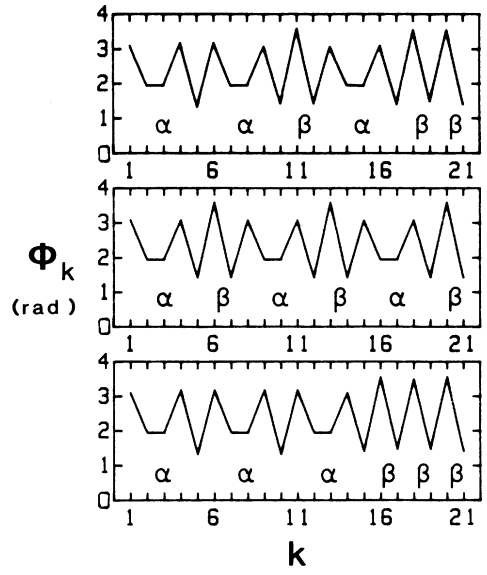

FIG. 14. Examples of stable heteroclinic structures consisting of α and β structures. $N=21$, $P=5$, $B=0.3$, and $\phi_0=0$.

shown in Fig. 9(b). The transition from (a) to (b) in Fig. 12 does not occur spontaneously, therefore an external perturbation (see Sec. V B) is needed to induce such a transition. On the other hand, the structure shown in Fig. 12(b) is found to be unstable and spontaneously undergoes transition to the structure shown in Fig. 12(c) based upon the numerical experiment. As a consequence, Fig. 12(a) represents the minimum distance between two kinks. From an extensive numerical simulation we confirmed that even if the spatial structure contains many kinks, the minimum distance mentioned above is the fundamental unit for an arbitrary pair of kinks to be able to exist stably. Thus the following rule is obtained.

Rule. Consider the α structure which contains a kink and is formed with 5 lattice sites and the β structure which is a fundamental unit of period-2 cycle structure as shown in Fig. 13. Structures which are obtained by arbitrary combination of α and β are dynamically stable.

Figure 14 shows examples of such structures.

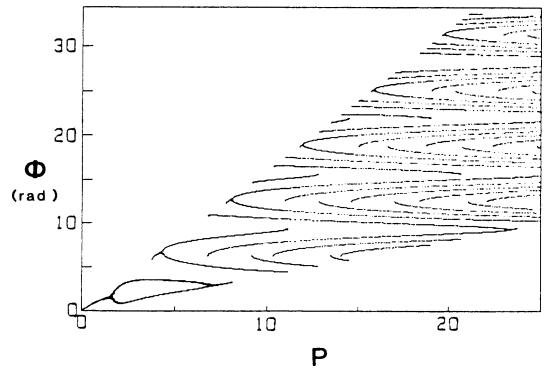

FIG. 15. Multistable structure of period-2 cycle solutions as a function of P. $B=0.3$ and $\phi_0=0$. Period-1 cycle solutions are also shown.

3. *Interheteroclinic structures*

The heteroclinic chaos structure which is produced within one period-2 cycle structure has been discussed so far. This structure is referred to as an "intraheteroclinic structure." If P is large enough, there are many dynamically stable period-2 cycle structures coexistent at a fixed value of P, as shown in Fig. 15. This is because the inverse function $f_P(\phi)^{-1}$ has many branches with respect to a slight change in ϕ. The intraheteroclinic structures exist within each period-2 cycle branch. Multifurcated structures, which are seen at each step of hysteresis in Fig. 4(b) represent such intraheteroclinic structures; the different steps correspond to different period-2 cycle structures.

In addition to the intraheteroclinic structure, an "interheteroclinc" chaos orbit, which connects different period-2 cycle structures, exists in our system. Examples are shown in Fig. 16. These structures are dynamically stable, although their dynamic stability is found to be weak compared with intraheteroclinic structures. The interheterostructure enables the spatial structure to wander between many period-2 cycle branches. This means that very irregular spatial structures may be realized in the high-P regime. A part of the fully chaotic structure which is seen in Fig. 5(b) can be boiled down to these interheteroclinic structures.

The structures which have been discussed so far are "interface" solutions switching between the same or different period-2 cycle solutions regardless of whether it is an intra- or an interheteroclinic structure. However, spatial chaos structures cannot always be explained only by the combination of these interface structures. In sufficiently-large-P regions, spatially unstable and temporally stable fundamental periodic solutions are not restricted to the period-2 cycle solution. In other words, chaotic patterns, which make rounds between an ex-

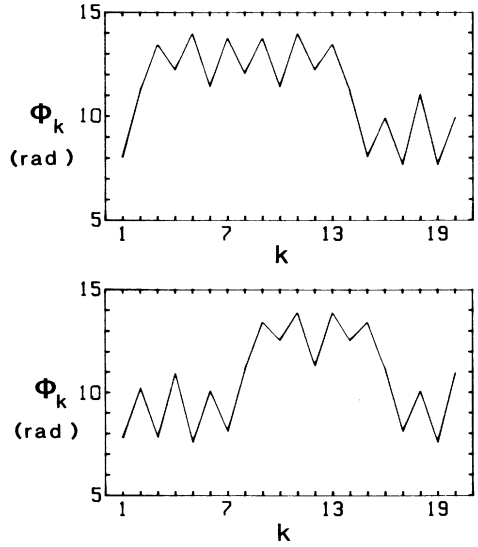

FIG. 16. Examples of interheteroclinic structures. $N=20$, $B=0.3$, $\phi_0=0$, and $P=10$.

tremely large variety of different fundamental periodic structures, exist stably in time. To indicate this, one should examine dynamically stable spatial structures by reducing the system size, i.e., N, such that intra- or interheteroclinic structures cannot be inserted into the chain. As will be shown in Appendix C, various dynamically stable spatial patterns exist in a sufficiently-small-N system in high-P regimes. It is no longer sufficient to say that these structures are formed of period-2 cycle structures. With an increase in P, the number of coexisting spatial patterns increases.

One of the interesting problems in spatial chaos is how transitions between these spatial patterns take place as a result of external perturbations. In short, a network structure involving various patterns, which is formed by external perturbations, is an interesting problem to investigate. Appendix C attempts to describe such a network structure. This problem is important from the practical view point of controlling the transition between different spatial patterns. Relating subjects will be described in Sec. V B.

V. COOPERATIVE FUNCTIONS

In this section, we describe cooperative phenomena in both unidirectional and bidirectional interaction schemes in terms of applicability to signal processing as well as to spatial chaos memory.

A. Domino dynamics in unidirectional coupling

In unidirectional coupling, dynamically stable spatial structures are restricted to spatially stable periodic solutions, and spatial chaos structures are not realized as stable stationary solutions. However, if the system is operated in a relatively low input intensity regime, it exhibits some interesting cooperative dynamics which can be applied to novel all-optical signal processing, including all kinds of multivibrator operations, flip-flops, and a complete set of logic gate operations.[16,17] If the excitation intensity A is small enough, the period-1 cycle solution, i.e., the trivial uniform solution, $\bar{\phi}_k=\bar{\phi}$, which continues to $\bar{\phi}_k\to 0$ at $A\to 0$, is obtained from Eq. (18) as

$$\bar{\phi}=A^2[1+2B\cos(\bar{\phi}+\phi_0)] . \tag{32}$$

Due to the existence of the cosine function, output $\bar{\phi}$ exhibits a multivalued function of A^2. This phenomenon is nothing more than an ordinary dispersive bistability (multistability). Of course, the uniform solution exhibits spatial period-doubling bifurcation when A^2 is increased and period-doubled structures appear. However, the bistable region always exists and the system can be operated as a bistable device. Figure 17 shows examples of the input versus output characteristics for different cell number N, assuming $B=0.2$ and $\phi_0=0$. Dashed curves indicate unstable branches. It is clear from the figure

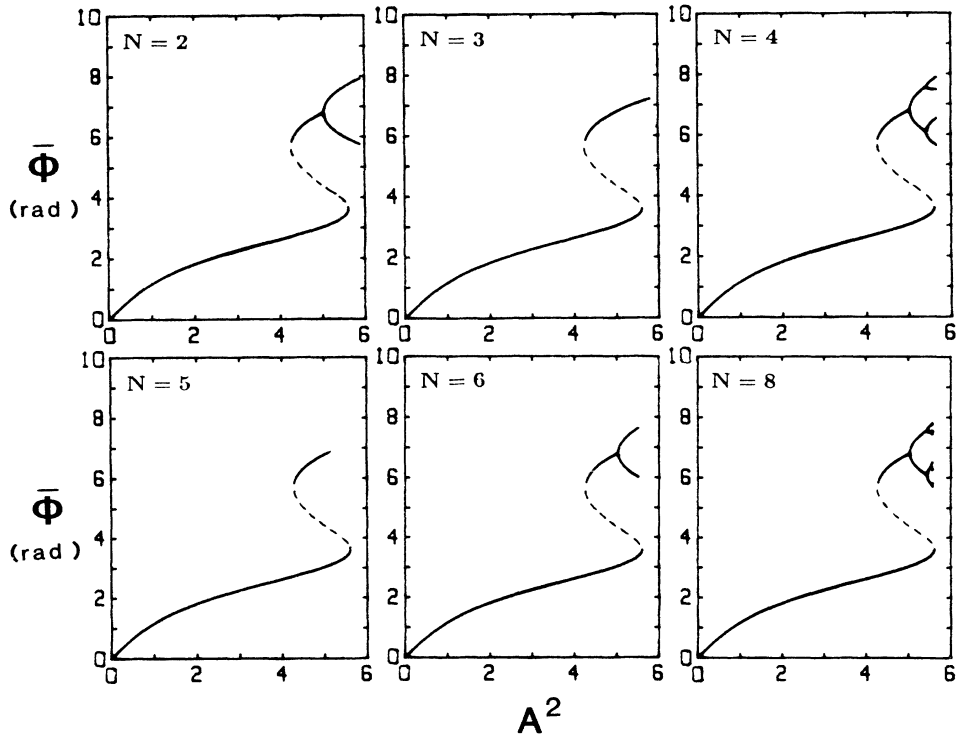

FIG. 17. Stationary solutions $\bar{\phi}_k$ as a function of input power A^2 for uniform excitations in the case of unidirectional interaction. $B=0.2$ and $\phi_0=0$. Stationary solutions corresponding to $S(p)$ $(p\neq 1)$ are omitted for brevity.

that an S-shaped bistable region appears just before the spatial period doubling takes place. If the system is operated as a bistable device in the hysteretic bistable region which has the spatial period-doubling regime on the upper branch, interesting cooperative dynamics, which will be discussed below, are expected to take place.

Assume that $N \gg 1$ and the system is set on the upper state ϕ_u of the S-shaped bistable region (see the regime $4.3 < A^2 < 5.7$ in Fig. 17.) and a single cell ($k=1$) is excited by an optical pulse A_p^2 superimposed on the input bias A^2. Then, ϕ_1 tends to relax to a new "destination"

$$\phi_1^* = f_F^{(1)}(\phi_u) = A_1^2[1+2B\eta_F^{(1)}\cos(\phi_u+\phi_0)] \equiv A_1^2 g^{(1)}(\phi_u) \quad (A_1^2 = A^2 + A_p^2)$$

roughly within a τ period. When ϕ_1^* is realized, then the destination toward which the second cell tends to relax is determined by $\phi_2^* = A^2 g^{(2)}(\phi_1^*)$. In this way, ϕ_k of the following cells "falls down" successively in domino fashion toward destinations determined by the mapping rule $\phi_k^* = A^2 g^{(k)}(\phi_{k-1}^*)$. The behavior of destinations of such domino dynamics is classified into three cases depending upon how A_p^2 is assigned: (1) all ϕ_k^* remain in the upper branch, (2) all ϕ_k^* switch down to the lower branch cooperatively, or (3) all ϕ_k^* goes up and down between the upper and lower branches. Any of these three classes can be selected by choosing the excitation strength to a $k=1$ cell which is determined by the relation shown in the map in Fig. 18(a), where $A^2(\text{bias}) = 4.5$, $B = 0.2$, and $\phi_0 = 0$ are assumed (see Fig. 17). Case (1) is realized in regions A and D, (2) is realized in region B, and (3) takes place in region C in Fig. 18(a). Corresponding to each of the three cases, the dynamics of our system differ: (1) $\phi_k(t)$ remains in the upper branch, (2) $\phi_k(t)$ switches down toward the lower branch, and (3) $\phi_k(t)$ exhibits up-down pulsation at every round trip (astable multivibration). On the other hand, when all cells are initially in the lower state ϕ_l, dynamics can also be classified into three other categories: (1) all $\phi_k(t)$ remain in the lower branch in region A and B of Fig. 18(a), (2) all $\phi_k(t)$ exhibit astable multivibration in region C, and (3) all $\phi_k(t)$ switch up to the upper region cooperatively in region D. The details of the operation principle in regions B and C are explained in Appendix B.

In order to confirm the above dynamics, numerical simulations are carried out using Eqs. (13)–(15), where $A_B^{(k)} = 0$, $N = 6$, $A^2 = 4.5$, $B = 0.2$, and $\phi_0 = 0$ are assumed. Results for the former case are depicted in Fig. 18(b). These results clearly reproduce the analytical prediction. (Results for the latter case also reproduce three relaxation dynamics, although they are not shown).

Next, let us discuss an all-optical flip-flop operation discovered in the present system. In ordinary bistable devices, such operations are performed by setting the system within the hysteretic region and by applying trigger pulses. In the all-optical operation, such operations are basically impossible, since one needs a "negative" optical pulse to realize off switching. This means that one has to prepare some kind of optical inverter in order to achieve successive on-off switching by trigger pulses, that is, flip-

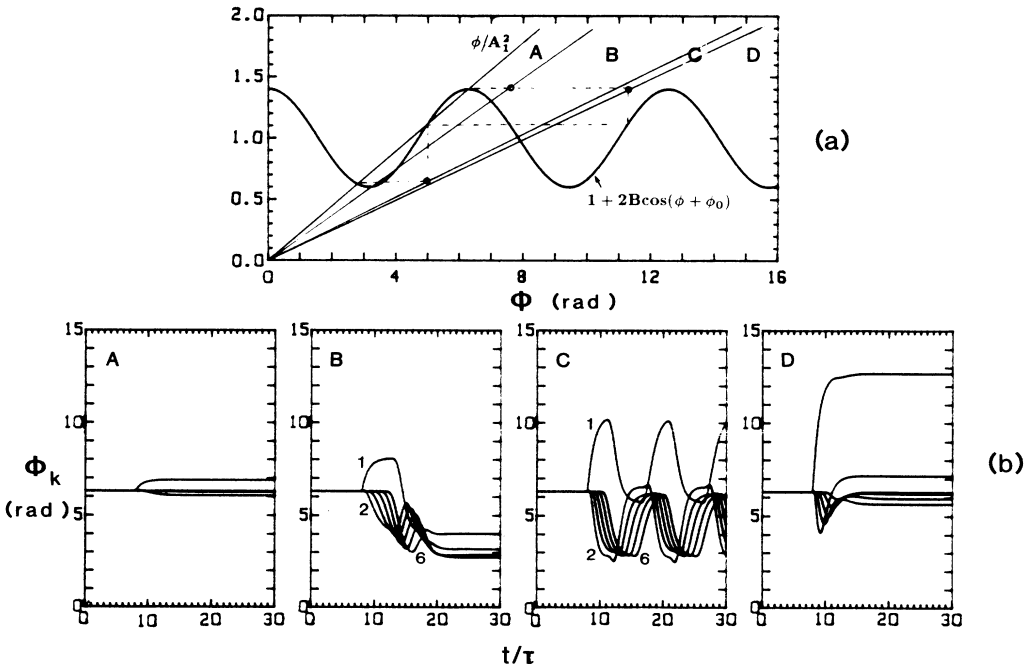

FIG. 18. Relaxation dynamics when single cell ($k=1$) is excited (nonuniform excitation). (a) Graphical solution for determining the class of relaxation dynamics, where $g(\phi) \equiv 1+2B\cos(\phi+\phi_0)$. (See Appendix B for details.) (b) Simulated temporal evolution of $\phi_k(t)$ for different regions A, B, C, and D, where the system is initially set on the upper branch of the hysteretic curve. $N=6$, $B=0.2$, $A^2(\text{bias}) = 4.5$, and $\phi_0 = 0$. Region A, $A_p^2(\text{pulse intensity}) = 0.5$; B, 1.5; C, 3.5; and D, 5.5.

flop or bistable multivibrator operations. (In optoelectric hybrid bistable devices, such operations have been demonstrated by employing optoelectrical inverters.[18,19])

On the other hand, the present distributed-element system can successfully provide such all-optical flip-flop functions by applying trigger optical pulses with finite pulsewidth to a single cell. It is easy to see that A_p^2 of the trigger pulse should be set in region B or C to realize an off switch and in region C or D to realize an on switch. To achieve the flip-flop operation, however, there exists a minimum duration time for the trigger pulse. The minimum trigger pulse cutoff timing is determined such that the greater portion of ϕ_k has already crossed the saddle at the trailing edge of the trigger pulses. Such a "majority" rule concept is easily understood and is reasonable in terms of domino dynamics. Numerical results are depicted in Fig. 19, where $N=6$, $A^2=4.5$, $B=0.2$, $\phi_0=0$, and $A_p^2=8$ are assumed. The majority rule is well reproduced by the simulation for both on and off switching.

B. Spatial chaos memory in bidirectional coupling

1. Capacity of spatial chaos memory

As was discussed in Sec. IV B, spatially unstable chaotic solutions are dynamically stabilized in the case of bidirectional coupling by the local feedback mechanism. From the viewpoint of memory function, this fact has a very important meaning: The existence of chaotic spatial solutions implies that the number of spatially unstable periodic solutions (with period N) increases exponentially with the number of cells N, i.e., $\exp(hN)$, where h is the topological entropy. In short, the memory capacity of $C=\log h/\log 2$ bit [which is derived from $2^{CN}=\exp(hN)$] is created per unit cell if we assume that all the periodic solutions are dynamically stable. In the present system, however, periodic solutions are not always dynamically stable, as discussed in Sec. IV B. Therefore $\log h/\log 2$ gives the theoretical upper limit of memory capacity. In our system, at least all spatial structures which are constructed of arbitrary combinations of α and β structures, are found to be dynamically stable, where α and β structures are formed of five and two cells, respectively. This fact ensures memory capacity of at least $\frac{1}{7}$ bits/cell. That is, the memory capacity of our system C (bits/cell) is evaluated as

$$\tfrac{1}{7} \le C < \log h/\log 2 \text{ bits/cell} . \tag{33}$$

This value seems to be not so large. However, the important point is that the memory function has been cooperatively created in our system by introducing the bidirectional interaction between cells which do not possess any memory function when the coupling is absent.

2. Assignment to desired spatial chaos patterns

Is it possible to assign the desired spatial patterns to our system? If we restrict the spatial patterns to the structures which are formed of α and β structures, it is quite easy to write any spatial patterns using the following methods.

In one method, first, the trivial period-1 cycle structure is realized by setting the system to the low-P regime. Then, a weak perturbation which has the same spatial pattern as the desired pattern is applied to the control parameter of each cell and P is increased to the multifurcated region. The linear phase shift $\phi_0^{(k)}$ or the input intensity to each cell $A_F^{(k)2}$ (or $A_B^{(k)2}$) is effective as a control parameter to be modulated. For example, let us consider the case that the linear phase shift is modulated. The seed $\delta\phi_i$ is assumed to be applied to ϕ_0 of each cell, where i is the cell number to be assigned. Then $\delta\phi_i$, which has the α-binary characteristic [$+--+-$ in Fig. 13(a)], is applied to five cells which an α structure should be assigned. As for β structures, the β-binary characteristic [$+-$ in Fig. 13(b)] is applied to two cells. Then, P is in-

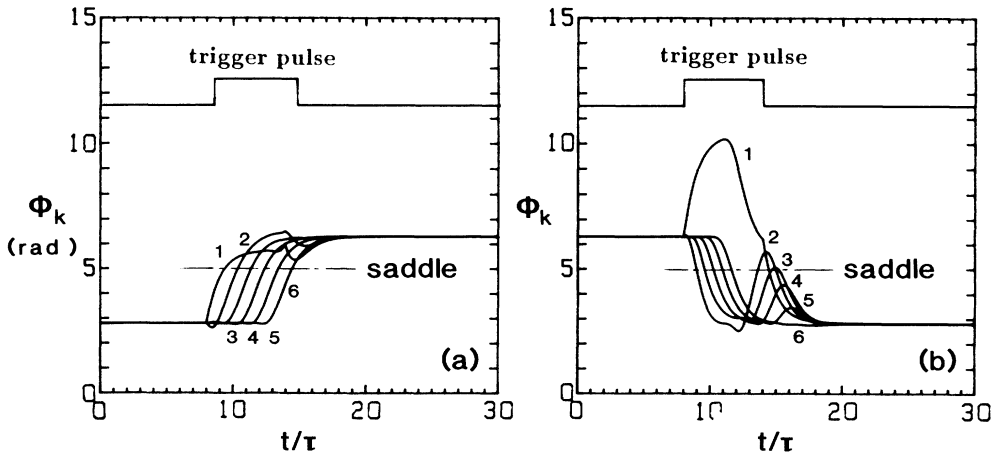

FIG. 19. All-optical flip-flop operation. A^2(bias)$=4.5$, $A_p^2=3.5$, $\Delta t/\tau$(pulsewidth)$=6$, $N=6$, $B=0.2$, and $\phi_0=0$. (a) On switching and (b) off switching.

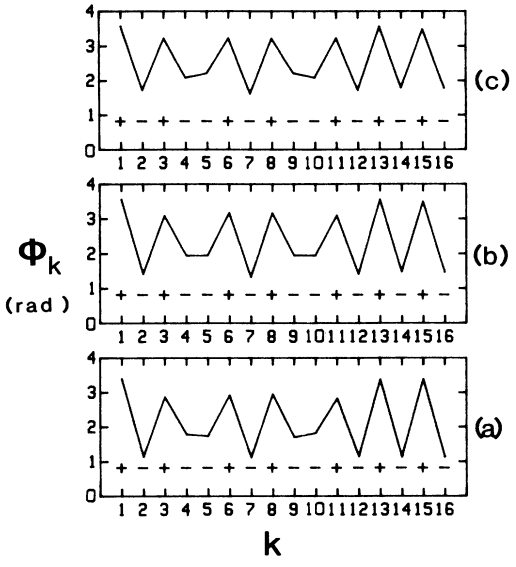

FIG. 20. Assignment to a desired spatial chaos pattern by modulating the linear phase shift ϕ_0. $N=16$, $B=0.3$, and $\phi_0=0$. (a) $P=2.7$, (b) 3.3, and (c) 4.0.

creased to the multifurcated region. By these processes, the desired structures can be assigned to desired positions. Once the desired patterns are realized, these patterns are frozen even if the perturbation is removed, and they are found to be quite stable against external random noise. Figure 20 shows the assigned spatial patterns obtained at different P values.

Let us consider another method. We showed that period-2 cycle structures (for even N) or period-2 structures into which a kink is inserted (for odd N) are the most stable ground states in the multifurcated region, i.e., $P>P_c$. It is possible to directly assign the desired spatial patterns consisting of α and β structures. In this method, the "ground-state" structures are realized at first by increasing P beyond P_c. Then, a perturbation which has binary characteristics corresponding to the desired spatial patterns is applied to the linear phase shift ($\phi_0^{(k)}$) or to the input intensity ($A_F^{(k)2}$ or $A_B^{(k)2}$) in the form of a *trigger pulse* with a finite pulsewidth. This method requires relatively strong perturbations compared to the former method, but, the spatial information input to the trigger pulses can be easily memorized as spatial patterns.

3. *Switching between desired patterns: Flexibility of spatial chaos memory*

Once the desired spatial patterns are realized, switching to different spatial patterns is easily achieved by applying a perturbation which has the same binary characteristics as the new patterns to the linear phase shift ($\phi_0^{(k)}$) or to the input intensity ($A_F^{(k)2}$, $A_B^{(k)2}$) in the form of trigger pulses as described in Sec. V B 2. With this perturbation, the old pattern makes a transition to a new one. There are thresholds for the amount of perturbation which must be overcome in order to make transitions. The threshold intensity depends upon the duration of the trigger pulse, and has been found to decrease in proportion to $(\Delta t/\tau)^{-1}$ (Δt is the pulsewidth). In both cases of the modulation of $A_{F,B}^{(k)2}$ and $\phi_0^{(k)}$, the threshold is as quite small (on the order of 10^{-2}) if the pulsewidth is much longer than the relaxation time of the system τ. Our system is distinctive in the sense that the transition between realizable *qualitatively different spatial patterns* can be performed quite easily by a slight modulation of the control parameter. In other words, the memory function of our system is rich in *flexibility*.

Let us examine such a phenomenon in the simplest case in more detail. If we deal with switching between structures which have the same number of α and β structures, this switching process is realized by combining several shifting operations on the α structures along the chain. Consider the single shifting operation, which is an elementary process. As discussed in Sec. IV B, this operation is realized most easily by shifting the kink along the "steepest descent" path which passes through the b-type kink state as in Fig. 11. Referring to Fig. 11, let us investigate further. If we modulate ϕ_0 (or A_F^2) according to the above-mentioned rule, it is possible to control the system's movement along this path. In the present case, the modulation of ϕ_0, which has the binary characteristics of the desired structure [Fig. 10(a)], should be $+\delta\phi_0$ to ϕ_1 and $-\delta\phi_0$ to ϕ_2. Such modulations are easily understood to move the system along the steepest descent. Figure 21 shows the relation between $\delta\phi_0$ (applied) and period Δt which is required for the system to cross over the saddle point. If $\delta\phi_0$ is sufficiently large, $\Delta t \sim \delta\phi_0^{-1}$. This suggests that the motion along the steepest descent, which is induced by the modulation of ϕ_0, takes place according to $\dot{s}=\delta\phi_0$ (driving force), where s is the distance from stable kink state a (in Fig. 11) measured along the steepest descent. Formally in the limit of $\delta\phi_0\to 0$, the motion becomes a "free motion" (i.e., $\dot{s}=0$). This suggests that the steepest descent is extremely flat.

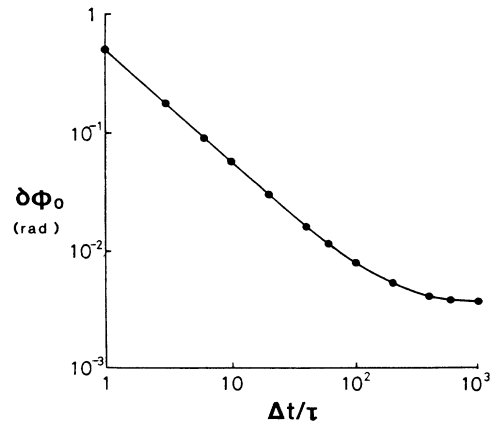

FIG. 21. Relation between the modulation amplitude $\delta\phi_0$ and period $\Delta t/\tau$ which is required for the system to cross over the saddle point. Adopted parameters are the same as those for Fig. 11.

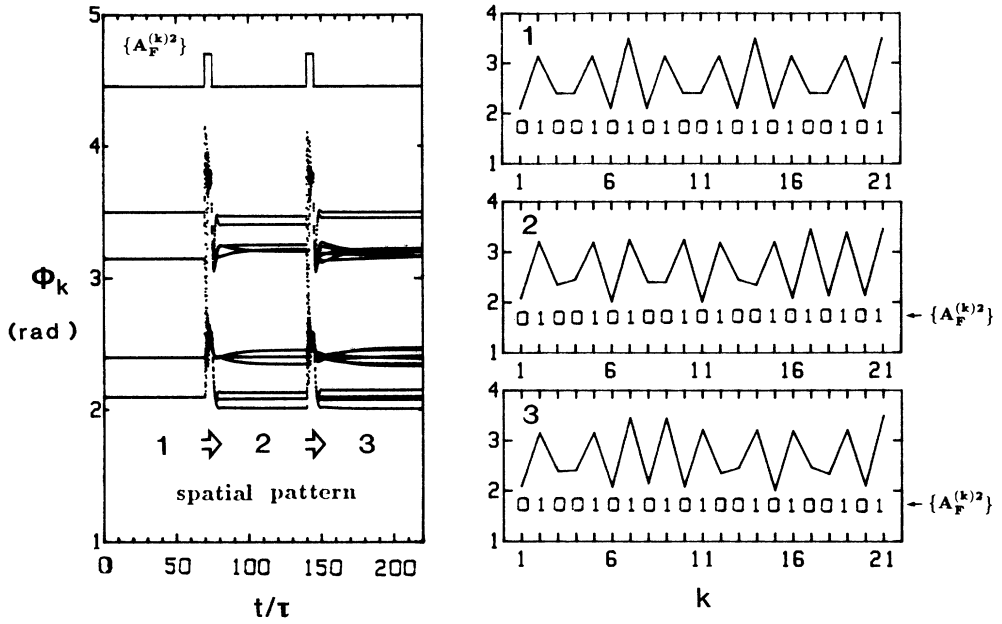

FIG. 22. Switching between desired patterns indicating a rewritable spatial chaos memory. Input signal $A_p^{(k)2}(k=1,2,\ldots,N)$ having binary characteristics is superimposed to the bias input $A_F^2=2.5$, where $A_B^2=2.5$ ($P=5$). In the binary characteristics shown in (b), "1" means that $A_p^{(k)2}=0.5$ and "0" means $A_p^{(k)2}=0$. $N=21$, $B=0.3$, and $\phi_0=0$. (a) Temporal evolution of $\phi_k(t)$ and (b) spatial arrangement of memorized patterns.

In the limit of $\delta\phi_0\rightarrow 0$, however, deviation from the rule $\Delta t \propto \delta\phi_0^{-1}$ begins to occur. Then, the "free motion" comes to be interrupted by the potential barrier and Δt goes to infinity at the critical value $\delta\phi_{0c}$. This value $\delta\phi_{0c}$ is extremely small (on the order of 3×10^{-3}). From this value, the potential barrier height at the saddle point ΔE_s can be evaluated. The ΔE_s value can be determined from the product of the critical perturbation strength, $\delta\phi_{0c}$ and the distance between the saddle point and the stable kink state in the Γ space which is given by $\Delta\phi_s$ of Fig. 11, that is, $\Delta E_s \sim \delta\phi_{0c}\Delta\phi_s \sim 10^{-3}$. Therefore ΔE_s is extremely small. This implies that if switching between the chaos patterns which have the same number of α and β structures is governed by the above-mentioned elementary process, these spatial chaos patterns are connected by the extremely "flat" steepest descent passing through the saddle point with an extremely low potential barrier. This may be a reason for the "flexibility" of our system. The coded modulation of ϕ_0 or A^2 results in a transition to a new chaotic pattern along a steepest descent.

Figure 22 shows an example of the switching process, where perturbations are applied to $A_F^{(k)2}$ in the form of trigger pulses. Rewritable spatial chaos memory is found to be achievable.

VI. SUMMARY AND OUTLOOK

Chaos is a complex behavior which is derived from a simple rule. If we can apply this aspect, it seems possible to realize complex functions by a simple device. For example, chaos possesses an ability to produce a variety of temporal patterns. If we use this ability, it might be possible to construct a memory element which stores complex information. This idea is the basic motivation of the present work. Unfortunately, the ability to produce various temporal patterns induces transitions between the produced patterns, and makes it impossible to distinguish them. On the other hand, there exists a possibility to stablize produced patterns dynamically if chaos is created in the space domain instead of in the time domain. The problem is whether it is possible to construct a device which can produce dynamically stable spatial chaos by utilizing a nonlinear optical system far from thermal equilibrium.

In this paper, we have discussed the stability and dynamic functions of spatial chaos which is produced cooperatively in the proposed collective nonlinear optical element system. The individual elements do not show any nontrivial properties in the absence of coupling between them. If coupling by laser light is introduced, the coupled system exhibits not only spatial chaos but also a variety of cooperative behavior.

If the coupling is unidirectional, it is easy to understand that there exist spatial chaos solutions in our system. Unfortunately, these spatial chaos structures are almost dynamically unstable since the spatial instability is converted into dynamic instability straightforwardly. However, if we apply the cooperative properties (domino dynamics) in the case of unidirectional coupling, novel forms of optical signal processing, including all-optical switching, multivibrator operations, and flip-flop operations can be realized.

As for bidirectional coupling, the dynamics drastically change. If the coupling exceeds the threshold, spatial

chaos solutions are dynamically stabilized over a wide range of input light intensity. In isolation, each element possesses only trivial properties. However, optical coupling gives each element in the system memory function having a finite capacity per unit element. Spatial chaos is shown to be a heteroclinic chaos of unstable period-2 cycle solutions which are born via spatial bifurcation. If we utilize the simplest heteroclinic chaos, the desired spatial patterns can be assigned, and switching between chaos patterns can easily be performed. Moreover, switching between chaos patterns is possible using extremely weak signals. This fact suggests that the memory function of the present spatial chaos is superior to ordinary memory devices in terms of flexibility.

However, the proposed metaphorical system requires multiple nonlinear elements, and the realization of such behavior in practice will require sophisticated fabrication techniques because of the complex device configuration of the present system. In addition, the memory capacity seems to be not so large. The important point, however, is that spatial chaos in our system satisfies the minimum demand for information storage functions. This is why we regard the proposed system as a metaphoric model of spatial chaos memory. In the spatial chaos memory, the information storage is accomplished by spatial chaos patterns which are formed by the cooperative interaction between individual elements rather than by individual elements themselves. The memory function acquired by such a mechanism is expected to possess novel properties (e.g., flexibility).

A state of the nonlinear optical device is specified by the spatial configuration of the electric field which passes through the device. With proper device configuration, a spatially varying electric field can possess spatial chaos as stationary solutions. The simplest example of such a device may be the system proposed by Yumoto and Otsuka.[7] If the Yumoto-Otsuka spatial chaos has dynamic stability similar to our proposed device, their system will be applicable to a device which possesses a large memory capacity. To realize complex functions by applying the distinctive characteristics of chaos, the dynamic aspect of spatial chaos in a simpler system like that of Yumoto-Otsuka should be investigated extensively.

APPENDIX A: DERIVATION OF FUNDAMENTAL EQUATIONS

We factorize the electric field into slowly varying envelopes and carrier waves of frequency ω and wave number k ($\omega=ck$, c being the velocity of light),

$$\hat{E}(t,z)=\hat{E}_F(t,z)e^{i(\omega t-kz)}+\hat{E}_B(t,z)e^{i(\omega t+kz)}+\text{c.c.} , \tag{A1}$$

where the notations F and B indicate the components propagating in the forward and backward directions, respectively. If we assume rapid diffusion of the phase grating due to the formation of standing waves and suppose both adiabatic approximation and dispersive limit, the Maxwell-Bloch equations are considerably simplified and become equivalent to the following Maxwell-Debye equations without phase grating,

$$\left[\frac{\partial}{\partial z}+\frac{\partial}{\partial(ct)}\right]E_F=-\tfrac{1}{2}(\alpha+i\alpha')E_F+inE_F , \tag{A2}$$

$$\left[-\frac{\partial}{\partial z}+\frac{\partial}{\partial(ct)}\right]E_B=-\tfrac{1}{2}(\alpha+i\alpha')E_B+inE_B , \tag{A3}$$

$$\tau\left[\frac{\partial n}{\partial t}\right]=-n+q(|E_F|^2+|E_B|^2) . \tag{A4}$$

Here, $\alpha+i\alpha'$ is the complex linear absorption rate, n is the nonlinear refractive index, $E_{F,B}\equiv[(1-e^{-\alpha l})|n_2|k/\alpha]^{1/2}\hat{E}_{F,B}$ is the dimensionless electric field (n_2 being the quadratic coefficient of the nonlinear refractive index), τ is the medium response time, l is the cell length, and $q\equiv\text{sgn}(n_2)[\alpha/(1-e^{-\alpha l})]$.

Transforming the time-space coordinates $(t-z/c,z)\rightarrow(t,z)$ for the forward component and $(t+z/c,z)\rightarrow(t,z)$ for the backward component, and integrating over z for Eqs. (A2) and (A3) lead to the following formula:

$$E_{F,B}(t\pm z/c,z)=\exp[\pm i\Phi_{F,B}(t,z)]E_{F,B}(t,0) . \tag{A5}$$

The phase shift $\Phi_{F,B}$ is given by

$$\Phi_{F,B}(t,z)=(i\alpha-\alpha')z/2+\phi_{F,B}(t,z) , \tag{A6}$$

where $\phi_{F,B}(t,z)$ is the nonlinear phase shift

$$\phi_{F,B}(t,z)=\int_0^z n(t\pm z'/c,z')dz' . \tag{A7}$$

Equation (A5) tells us that the intensity $|E_{F,B}|^2$ decays exponentially (Beer's law),

$$|E_{F,B}(t\pm z/c,z)|^2=e^{\mp\alpha z}|E_{F,B}(t,0)|^2 . \tag{A8}$$

From Eqs. (A4)–(A8), the following equations are obtained:

$$E_F(t+l/c,l)=\exp\{-(\alpha/2)l+i[\phi_F(t,l)+\phi_0]\}E_F(t,0) , \tag{A9}$$

$$E_B(t+l/c,0)=\exp\{-(\alpha/2)l+i[\phi_B(t+l/c,l)+\phi_0]\}E_B(t,l) , \tag{A10}$$

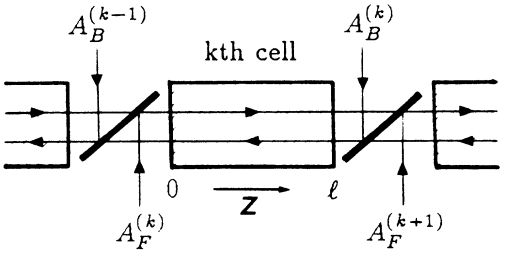

FIG. 23. Conceptual illustration of bidirectional coupling scheme.

$$\tau\left[\frac{\partial\phi_F(t,l)}{\partial t}\right]$$
$$=-\phi_F(t,l)+q[(1-e^{-\alpha l})/\alpha]|E_F(t,0)|^2$$
$$+q\int_0^l dz\, e^{-\alpha z}|E_B(t-2z/c+l/c,l)|^2\ , \tag{A11}$$

$$\tau\left[\frac{\partial\phi_B(t+l/c,l)}{\partial t}\right]$$
$$=-\phi_B(t+l/c,l)+q[(1-e^{-\alpha l})/\alpha]|E_B(t,l)|^2$$
$$+q\int_0^l dz\, e^{-\alpha z}|E_F(t-2z/c+l/c,0)|^2\ , \tag{A12}$$

where $\phi_0=(\alpha'/2)l$ is the linear phase shift.

A conceptual illustration of the bidirectional coupling scheme is shown in Fig. 23. Here, we rewrite the electric field, linear phase shift and nonlinear phase shift of the kth cell as $E_F(t,0)\to E_F^{(k)}(t)$, $E_B(t,l)\to E_B^{(k)}(t)$, $\phi_0\to\phi_0^{(k)}$, $\phi_F(t,l)\to\phi_F^{(k)}(t)$, and $\phi_B(t+l/c,l)\to\phi_B^{(k)}(t)$. Taking into account the boundary condition at the mirror, the following equations are derived from Eqs. (A9)–(A12):

$$E_F^{(k+1)}(t+l/c)=A_F^{(k+1)}$$
$$+\sqrt{R}\ \exp(-\alpha l/2)$$
$$\times\exp\{i[\phi_F^{(k)}(t)+\phi_0^{(k)}]\}E_F^{(k)}(t)\ , \tag{A13}$$

$$E_B^{(k-1)}(t+l/c)=A_B^{(k-1)}$$
$$+\sqrt{R}\ \exp(-\alpha l/2)$$
$$\times\exp\{i[\phi_B^{(k)}(t)+\phi_0^{(k)}]\}E_B^{(k)}(t)\ , \tag{A14}$$

$$\tau\left[\frac{\partial\phi_F^{(k)}(t)}{\partial t}\right]$$
$$=-\phi_F^{(k)}(t)+q[(1-e^{-\alpha l})/\alpha]|E_F^{(k)}(t)|^2$$
$$+q\int_0^l ds\, e^{-\alpha s}|E_B^{(k)}(t+l/c-2s/c)|^2\ , \tag{A15}$$

$$\tau\left[\frac{\partial\phi_B^{(k)}(t)}{\partial t}\right]$$
$$=-\phi_B^{(k)}(t)+q[(1-e^{-\alpha l})/\alpha]|E_B^{(k)}(t)|^2$$
$$+q\int_0^l ds\, e^{-\alpha s}|E_F^{(k)}(t+l/c-2s/c)|^2\ , \tag{A16}$$

where $A\equiv[(1-e^{-\alpha l})|n_2|k/\alpha]^{1/2}\hat{A}$ is the amplitude of the incident laser light (dimensionless) and R is the reflectivity of the mirror. If we define the coupling coefficient $B\equiv\sqrt{R}\,e^{-(\alpha l/2)}$ and transit time $t_R\equiv l/c$, Eqs. (7)–(10) are derived.

APPENDIX B: PRINCIPLE OF DOMINO DYNAMICS

1. Cooperative switching

As mentioned in Sec. V A, the input field to a specific cell should be slightly changed from the input field to other cells in order to realize the domino dynamics. This introduces the following cell dependence of coupling function:

$$f_F^{(k)}(\phi)=A_F^{(k)2}[1+2B\eta_F^{(k)}\cos(\phi+\phi_0)] \tag{B1}$$

via the two terms $A_F^{(k)2}$ and $\eta_F^{(k)}\equiv A_F^{(k-1)}/A_F^{(k)}$. The modulation due to the former term is essential for the operation of domino dynamics. To avoid nonessential complexity we approximate $\eta_F^{(k)}$ by 1 even if $A_F^{(k)}$ is modulated. Then the coupling function is expressed as $f_F^{(k)}\equiv A_k^2 g(\phi)$, where $g(\phi)=1+2B\cos(\phi+\phi_0)$.

Assume that $N\gg 1$ and that all the cells are set on the period-1 cycle structure on the upper branch, which is determined by $\phi_u=A^2 g(\phi_u)$. When the input light intensity of the first cell ($k=1$) is increased such that $A^2\to A_1^2$ ($A_1^2\in B$ regime), the destination of relaxation of ϕ_1 is changed from ϕ_u to $\phi_1^*=A_1^2 g(\phi_u)$. [See Fig. 24(a)]. As a result, ϕ_1 relaxes to ϕ_1^* and increases once as seen in Fig. 15(b). However, since ϕ_1^* belongs to the basin of attraction of the lower branch, the destination toward which the following cells tend to relax converges to the lower branch solution ϕ_l such that $\phi_2^*=A^2 g(\phi_1^*)$, $\phi_3^*=A^2 g(\phi_2^*),\ldots,$ as shown in Fig. 24(a). Therefore ϕ_N tends to relax to ϕ_N^*, which is very close to ϕ_l, and the destination of relaxation of ϕ_1 is then changed from ϕ_1^* to $\phi_1'^*=A_1^2 g(\phi_l)$. Since $\phi_1'^*$ belongs to the basin of attrac-

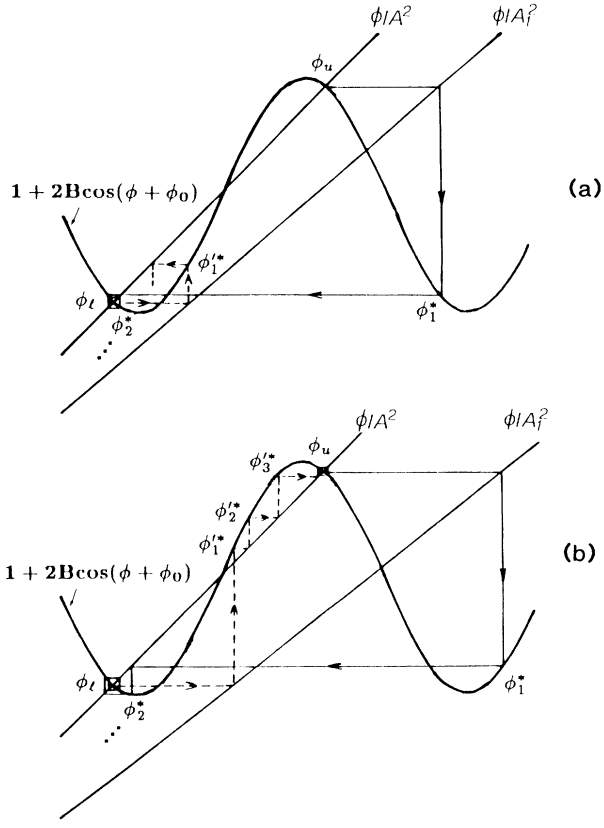

FIG. 24. Principle of domino dynamics. (a) Conceptual illustration of cooperative switching and (b) astable multivibrator operations.

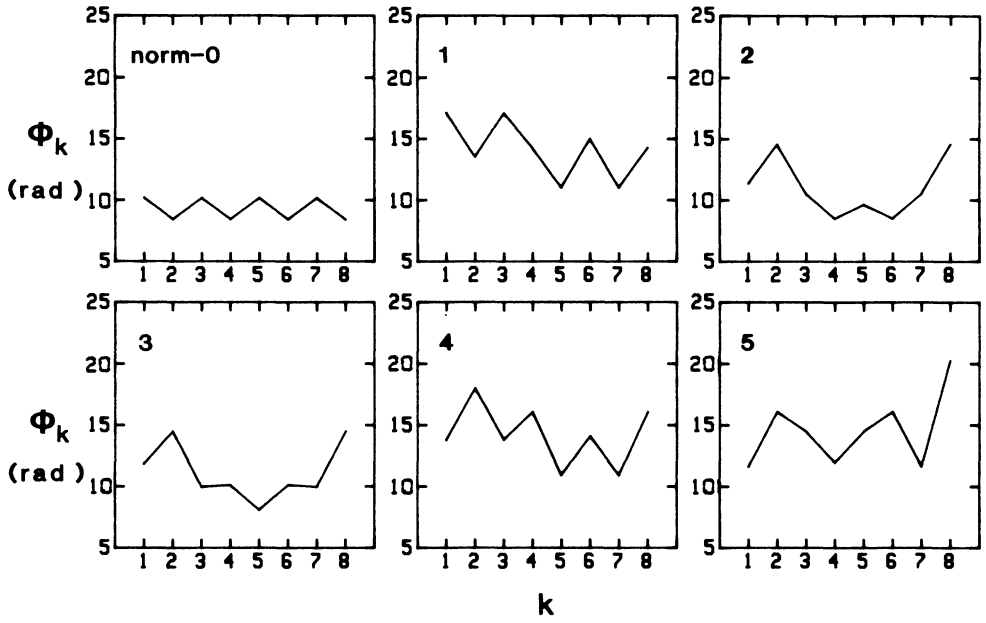

FIG. 25. Coexisting spatial patterns for $N=8$, $B=0.3$, $P=15$, and $\phi_0=0$.

tion of the lower branch [Fig. 24(a)] by the definition of region B, all the ϕ's are frozen to the stable spatial pattern $\bar{\phi}_1=A_1^2 g(\bar{\phi}_N)$, $\bar{\phi}_2=A^2 g(\bar{\phi}_1), \ldots, \bar{\phi}_N=A^2 g(\bar{\phi}_{N-1})$ and cooperative switching is realized.

2. Multivibrator operation

Let us choose A_1^2 within the C regime. All behavior in the first half is the same as that of (1), and the destinations of relaxation are changed to $\phi_1^*=A_1^2 g(\phi_u)$, $\phi_2^*=A^2 g(\phi_1^*), \ldots$. As a result, ϕ_1 increases once as seen in Fig. 15(b) and $\phi_2,\phi_3,\ldots,\phi_N$ relax to ϕ_l. The different dynamics arise in the latter half. Due to the definition of region C, the new destination of relaxation $\phi_1'^*=A_1^2 g(\phi_N)\simeq A_1^2 g(\phi_l)$ belongs to the basin of attraction of the upper branch [Fig. 24(b)]. Therefore, new destinations of relaxation of $\phi_2,\phi_3,\ldots,\phi_N$ are switched to the upper branch such that $\phi_2'^*=A^2 g(\phi_1'^*)$, $\phi_3'^*=A^2 g(\phi_2'^*), \ldots$, and relax successively toward ϕ_u as shown in Fig. 24(b). The same process occurs repeatedly hereafter and astable multivibrator operation takes place.

As emphasized at the beginning of this appendix, we used the approximation $\eta_F^{(k)}\approx 1$ throughout the above considerations. The effect of deviation of $\eta_F^{(k)}$ from 1 is by no means negligible, especially when B is very small (say, $B<0.1$). In this limit, the modulation effect reduces region B (i.e., cooperative switching), thereby widening region C (i.e., astable multivibrator operation). However, the modulation effect is not significant if B is not very small and therefore the above considerations are substantially correct.

APPENDIX C: DEVELOPMENT OF THE CONNECTIVITY BETWEEN SPATIAL CHAOS PATTERNS

In the bidirectionally coupling system, the number of dynamically stable frozen spatial patterns increases with

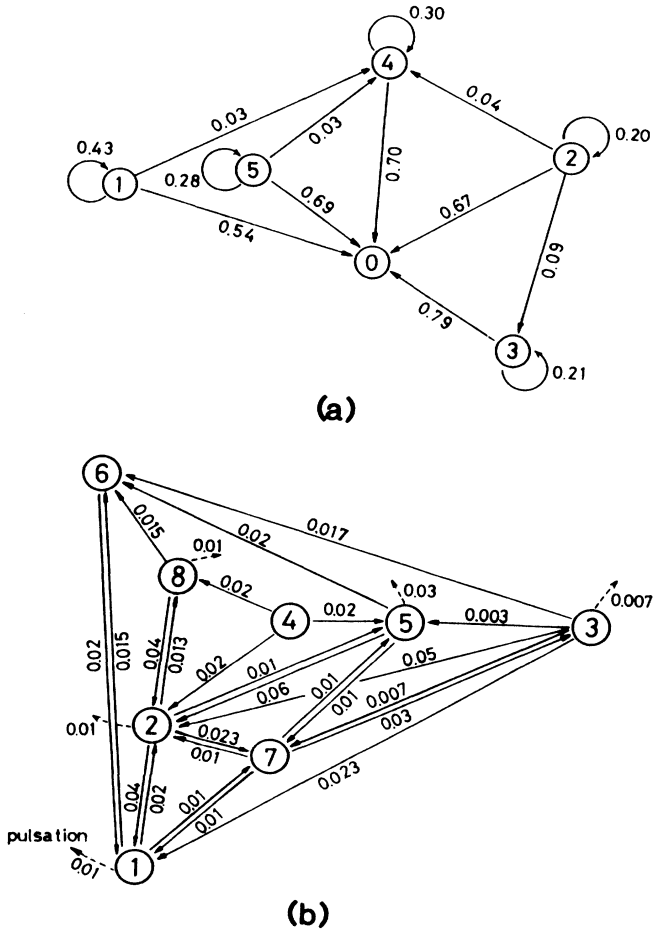

FIG. 26. Transition diagram between coexisting spatial patterns. $N=8$, $B=0.3$, and $\phi_0=0$. (a) $P=15$, and (b) $P=23$.

P, and finally these solutions are replaced by spatiotemporal chaos (STC) as was shown in Fig. 4(b). Stable frozen structures are considered to form local minima in Γ space. As P is increased, the number of local minima increases and the relation between these local minima will be much more complicated. In this appendix, let us discuss the *connectivity* between coexisting spatial chaos structures.

In a large-N system, an extremely large number of spatial chaos patterns appear. Therefore we assume a small-N system ($N=8$). Note that the fundamental structures including α and β have no meaning at all for such a small cell number. To categorize various coexisting structures, we define the norm which indicates a "distance" from the period-2 cycle structure, $D=[\sum_{k=1}^{N}|\cos(\phi_k)-\cos(\phi_{k-2})|^2]^{1/2}$.

Let us perform the following manipulation to characterize the connectivity quantitatively. Assume the system is set to the pattern i initially. Next, the linear phase shift ϕ_0 of all the cells is uniformly modulated pulsewise, i.e., $\phi_0 \rightarrow \phi_0+\delta\phi(t)$, where the modulation width is set as $0<\delta\phi<2\pi$. After that the system is left alone. We define the connectivity as follows: $T_{ij}=\delta\phi_{i\rightarrow j}/2\pi$. This connectivity gives the transition probability from i to j when uniform "error" is assumed to be introduced to the linear phase shift of all the cells. The *transition diagram* between patterns which have different norms can be described according to the connectivity T_{ij}.

Let us show an example for a relatively small P value ($P=15$). As shown in Fig. 25, there exist five patterns with different norms. The transition diagram between these patterns is depicted in Fig. 26(a). All the patterns are connected to the norm-0 pattern, i.e., a period-2 cycle structure with a large connectivity. This is reasonable since the period-2 cycle structure is a ground state in our system. However, the connectivity is weak as a whole and unidirectional. As a result, it is difficult to realize arbitrary patterns starting from one particular pattern in this case.

When P is increased, the situation greatly changes. Figure 26(b) depicts the transition diagram for $P=23$. In this case, there are nine different norm patterns including period-2 cycle (norm-0) patterns. Figure 26(b) omits the transition to norm-0 patterns. The distinctive feature is that the connectivity in the transition diagram becomes much stronger as a whole. Except for norm-4 patterns, any pattern can be realized starting from an arbitrary pattern. This means that the increase in P increases not only the number of spatial patterns but also the connectivity between different structures.

[1] H. M. Gibbs, *Optical Bistability: Controlling Light with Light* (Academic, New York, 1985).

[2] H. Kawaguchi, Opt. Quantum Electron. **19**, S1 (1987).

[3] J. J. Hopfield, Proc. Natl. Acad. Sci. U.S.A. **79**, 2554 (1982).

[4] Y. Owechko, E. Marcom, B. H. Soffer, and G. Dunning, Proc. SPIE **700**, 296 (1986).

[5] *Instabilities and Chaos in Quantum Optics,* edited by F. T. Arecchi and R. G. Harrison (Springer-Verlag, Berlin, 1987).

[6] Aubry, in *Solitons and Condensed Matter Physics,* edited by A. R. Bishop and T. Schneider (Springer-Verlag, Berlin, 1979), p. 264.

[7] J. Yumoto and K. Otsuka, Phys. Rev. Lett. **54**, 1806 (1985); K. Otsuka and J. Yumoto, Proc. SPIE **667**, 167 (1986).

[8] B. Daino, G. Gregori, and S. Wabnitz, J. Appl. Phys. **58**, 4512 (1985); Opt. Lett. **11**, 42 (1986); H. G. Winful, *ibid.* **11**, 33 (1986); G. Gregori and S. Wabnitz, Phys. Rev. Lett. **56**, 600 (1986); F. Matera and S. Wabnitz, Opt. Lett. **11**, 467 (1986); S. Wabnitz, Phys. Rev. Lett. **58**, 1415 (1987); A. Mecozzi, S. Trillo, S. Wabnitz, and B. Daino, Opt. Lett. **12**, 275 (1987); A. Mecozzi, S. Trillo, and S. Wabnitz, *ibid.* **12**, 1008 (1987); M. V. Tratnik and J. E. Sipe, Phys. Rev. A **35**, 2965 (1987); **35**, 2976 (1987); **36**, 4817 (1987).

[9] W. J. Firth, Phys. Lett. A **125**, 375 (1987).

[10] P. Davis and K. Ikeda (unpublished).

[11] P. Davis (unpublished).

[12] K. Otsuka and K. Ikeda, Phys. Rev. Lett. **59**, 194 (1987).

[13] K. Ikeda and M. Mizuno, IEEE J. Quantum Electron. **QE-21**, 1429 (1985).

[14] K. Ikeda, in *Coherence and Quantum Optics V,* edited by L. Mandel and E. Wolf (Plenum, New York, 1984), p. 875.

[15] J. Guckenheimer and P. Holmes, *Nonlinear Oscillations, Dynamical Systems, and Bifurcations of Vector Fields* (Springer-Verlag, Heidelberg, 1983), Chap. 5.

[16] K. Otsuka and K. Ikeda, Opt. Lett. **12**, 599 (1987).

[17] K. Otsuka, Electron. Lett. **24**, 800 (1988); Opt. Lett. **14**, 72 (1989).

[18] K. Okumura, Y. Ogawa, and H. Inaba, IEEE J. Quantum Electron. **QE-21**, 325 (1985).

[19] J.-M. Liu and Y.-C. Chen. IEEE J. Quantum Electron. **QE-21**, 298 (1985).

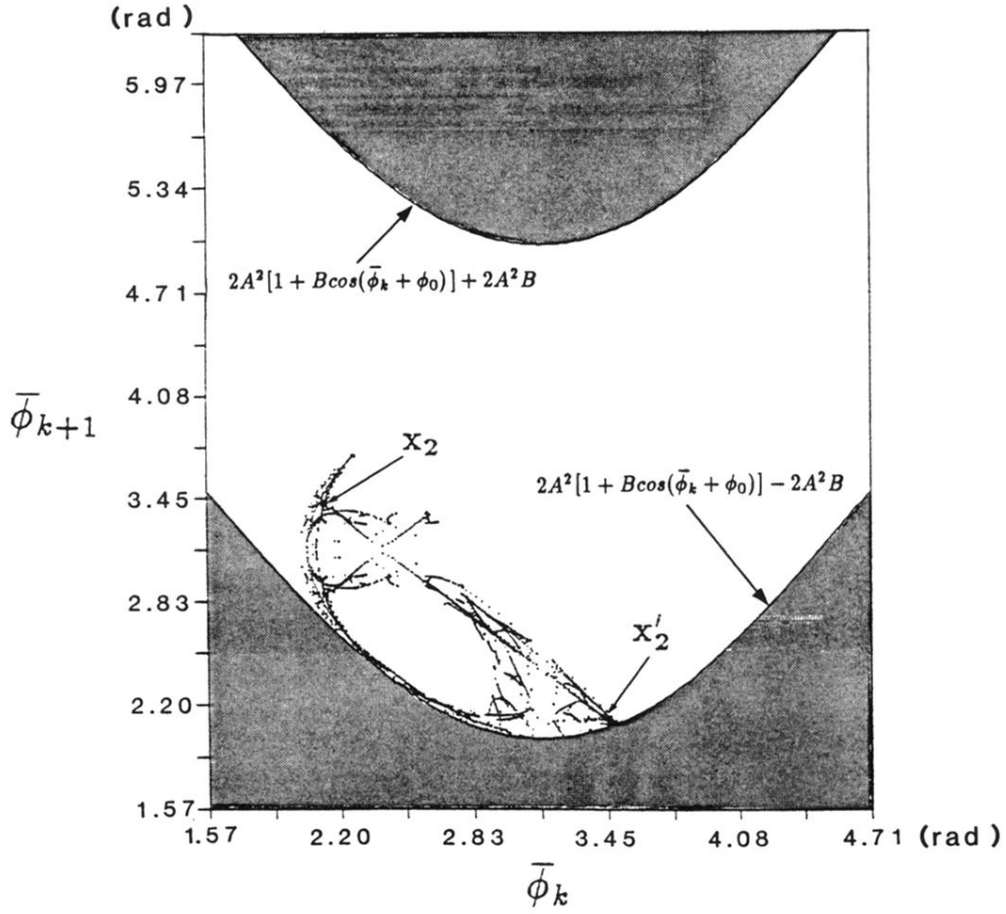

FIG. 7. Heteroclinic complex computed numerically based on the recursive relation of Eq. (24), where $P=5$, $B=0.3$, and $\phi_0=0$. Solutions cannot exist in the shadowed regions, since $-1\leq\cos(\bar{\phi}_{k+2}+\phi_0)\leq 1$. This structure is obtained by choosing the appropriate branch from among mapping solutions physically. Therefore this structure is considered to form part of the actual heteroclinic complex.